Article

Targeting a Novel KRAS Binding Site: Application of One-Component Stapling of Small (5−6-mer) Peptides

Gabriele Fumagalli, Rodrigo J. Carbajo, J. Willem M. Nissink, Jonathan Tart, Rongxuan Dou, Andrew P. Thomas,* and David R. Spring*

Cite This: *J. Med. Chem.* 2021, 64, 17287−17303

Read Online

ACCESS | Metrics & More | Article Recommendations | Supporting Information

ABSTRACT: RAS proteins are central in the proliferation of many types of cancer, but a general approach toward the identification of pan-mutant RAS inhibitors has remained unresolved. In this work, we describe the application of a binding pharmacophore identified from analysis of known RAS binding peptides to the design of novel peptides. Using a chemically divergent approach, we generated a library of small stapled peptides from which we identified compounds with weak binding activity. Exploration of structure−activity relationships (SARs) and optimization of these early compounds led to low-micromolar binders of KRAS that block nucleotide exchange.
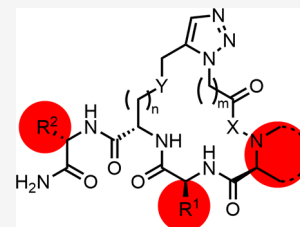
INTRODUCTION

RAS proteins, small guanosine triphosphatases (GTPases), act as molecular switches that are in an active conformation when they are bound to guanosine 5′-triphosphate (GTP) and become inactive when bound to guanosine diphosphate (GDP) following GTP hydrolysis. The RAS family includes three key proteins (HRAS, NRAS, and KRAS) that play a crucial role in cellular signaling driven by receptor tyrosine kinases, which can mediate a variety of key cellular outcomes including proliferation, differentiation, growth, apoptosis, and cell survival.[1,2] Activating mutations in RAS that favor the active GTP bound conformation and/or decrease its GTPase activity are common drivers of many cancers including pancreatic cancers, lung adenocarcinomas, and colorectal cancers.[3] KRAS is the most frequently mutated member of the RAS family found in tumors.[4] While the attractiveness of targeting RAS has been clear from a therapeutic and biological perspective, the identification of small molecule inhibitors has proven to be challenging due to the shape and size of RAS proteins and the lack of clearly defined pockets to which small molecules could bind with high-affinity binding. The nucleotide-binding site would represent one such pocket, but it presents its own unique challenges due to RAS proteins having a very high affinity for GTP and GDP, resulting in very strong competition for binding with a small-molecule inhibitor.[5] Thus, finding potent RAS inhibitors with drug-like properties has been a major challenge. However, in recent years, novel approaches to this problem have highlighted new binding opportunities. First, the specific and covalent targeting of the cysteine mutation in the KRAS G12C protein has delivered inhibitors that exploit binding to a cryptic pocket in the switch II region, which has led to the first approved therapy that directly targets KRAS (Sotorasib/AMG 510).[6] Another significant step forward in the area is the recent report of reversible RAS inhibitors that bind to a pocket between the

switch I and II regions. Initial binders were discovered through the application of a fragment screening approach that was optimized to give the potent, pan KRAS inhibitor BI-2852.[7] A third direct binding site on RAS has been identified by the Takeda group who reported the discovery of novel peptide inhibitors *via* random T7 phage-display library screening.[8] These peptides bind to the external face of the switch II region, and this binding site represents another potentially significant step forward in targeting RAS and in the identification of inhibitors to this important and previously undruggable target.[9] Further development of these peptide binders has recently been reported.[10]

Our own interest in this area originated from independent work to identify RAS inhibitory peptides following an approach related to that reported by the Takeda group,[8] through a collaboration between AstraZeneca and Pepti-dream.[11] This led to the identification of a series of peptides with nanomolar potency. Co-crystal structures of these peptides with KRAS[G12V] showed a binding interaction with RAS that is closely related to that reported by Sogabe et al. for the Takeda peptide KRpep-2d.[8] The key, common RAS binding interactions shown by these peptides are made by three hydrophobic peptide residues that bind to common sites on RAS, i.e., residues Pro6, Leu7, and Ile9 on structure KRpep-2d,[8] and corresponding residues Pro, Ile, and Leu in the AstraZeneca peptide (**1**) (Figure 1; key residues highlighted in purple). The importance of these binding interactions was
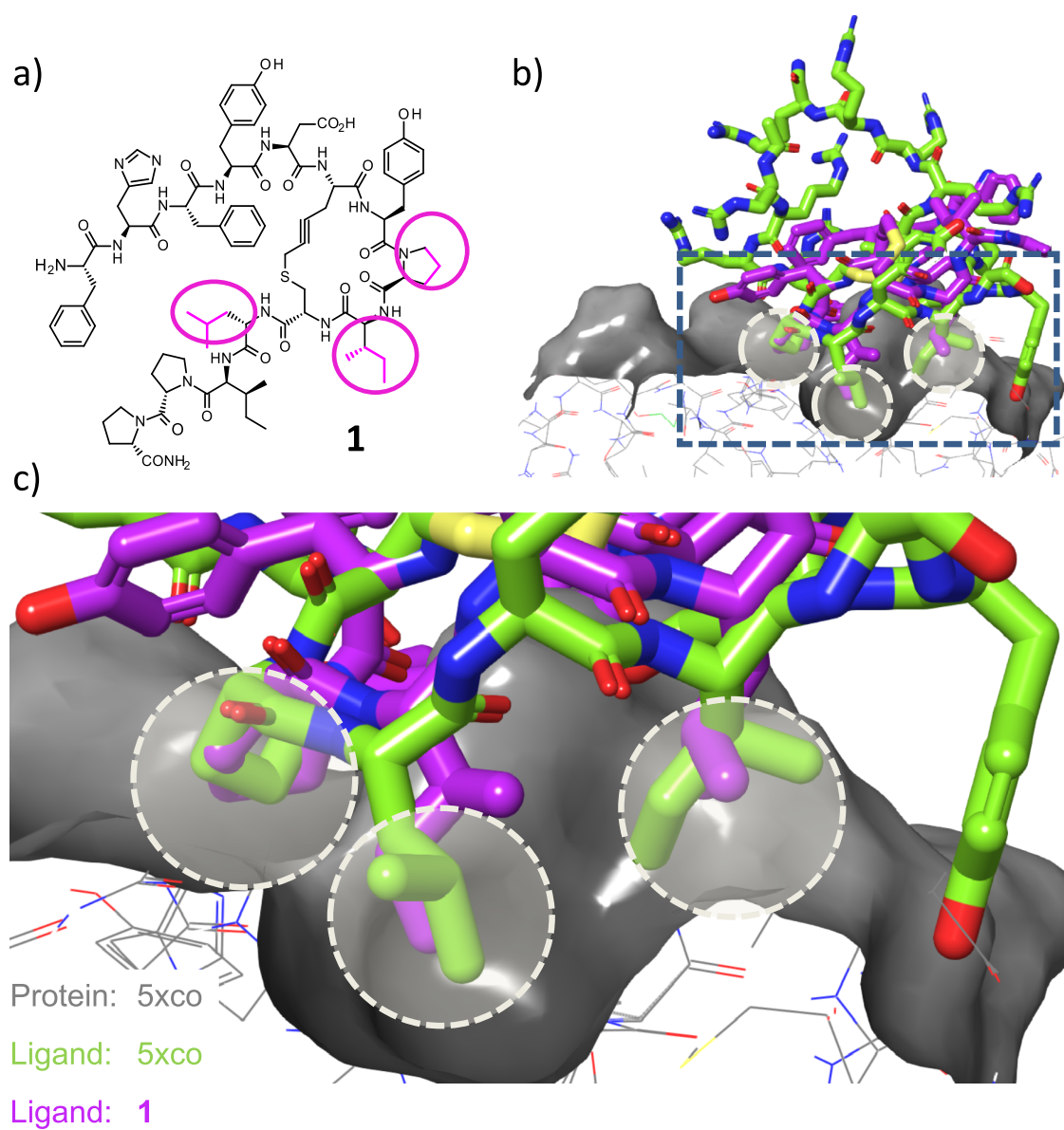
Figure 1. Initial peptide binder **1** and overlays with Takeda peptide KRpep-2d. (a) Structure of **1**. (b) Overlay of **1** (purple) from the crystal structure of the complex with KRAS[G12V] with the crystal structure of KRpep-2d (green) reported by Sogabe et al.[8] PDB accession code: 5xco. (c) Detail of overlay of **1** with KRpep-2d showing key hydrophobic RAS binding residues (circled).

confirmed by structural analysis of the binding modes of several peptides and general SAR for potent binding activity,[11] the result of which is consistent with the outcome of an alanine scan reported by the Takeda group.[8] While the original series of peptides, upon which this work is based, did contain acidic or basic residues that interacted with oppositely charged residues on the surface of RAS, there was no specific residue or charge−charge interaction that was consistently required for binding potency, and as these interactions were all solvent exposed, we judged them likely not to make a major contribution to binding affinity. Additionally, as the aim of this work was to identify smaller, more drug-like molecules, we aimed to avoid the inclusion of acidic or highly basic residues.

While novel peptide binders are relatively easy to discover and synthesize,[12] their properties are generally non-drug-like: low cellular permeability, low proteolytic stability, high clearance, and poor physicochemical profile.[13] Such issues limit the utility of the earlier peptide series, with the lack of

membrane penetration and cellular activity being major limitations. Various methodologies have been proposed to deal with a wide range of potential issues, e.g., introduction of D-amino acids to improve protease stability or addition of poly-arginine tags to improve cellular uptake.[14] In recent years, peptide stapling (linking together two side chains to generate a macrocycle) has established itself as a leading technology.[15] The introduction of a staple can "lock" the peptide in the active conformation and maintain helicity in smaller peptides, thus improving both the physicochemical profile (enhanced stability and permeability) and potency (reducing the entropic cost of binding).[15,16]

In the work described here, we sought to exploit a stapling approach on small core peptides, based on the macrocyclic motif of larger peptide binders, to improve properties and simplify the structures of these RAS binders. Compound **1** (Figure 1a) was selected as the prototype peptide for this work as it contains a constraining staple that guided the design
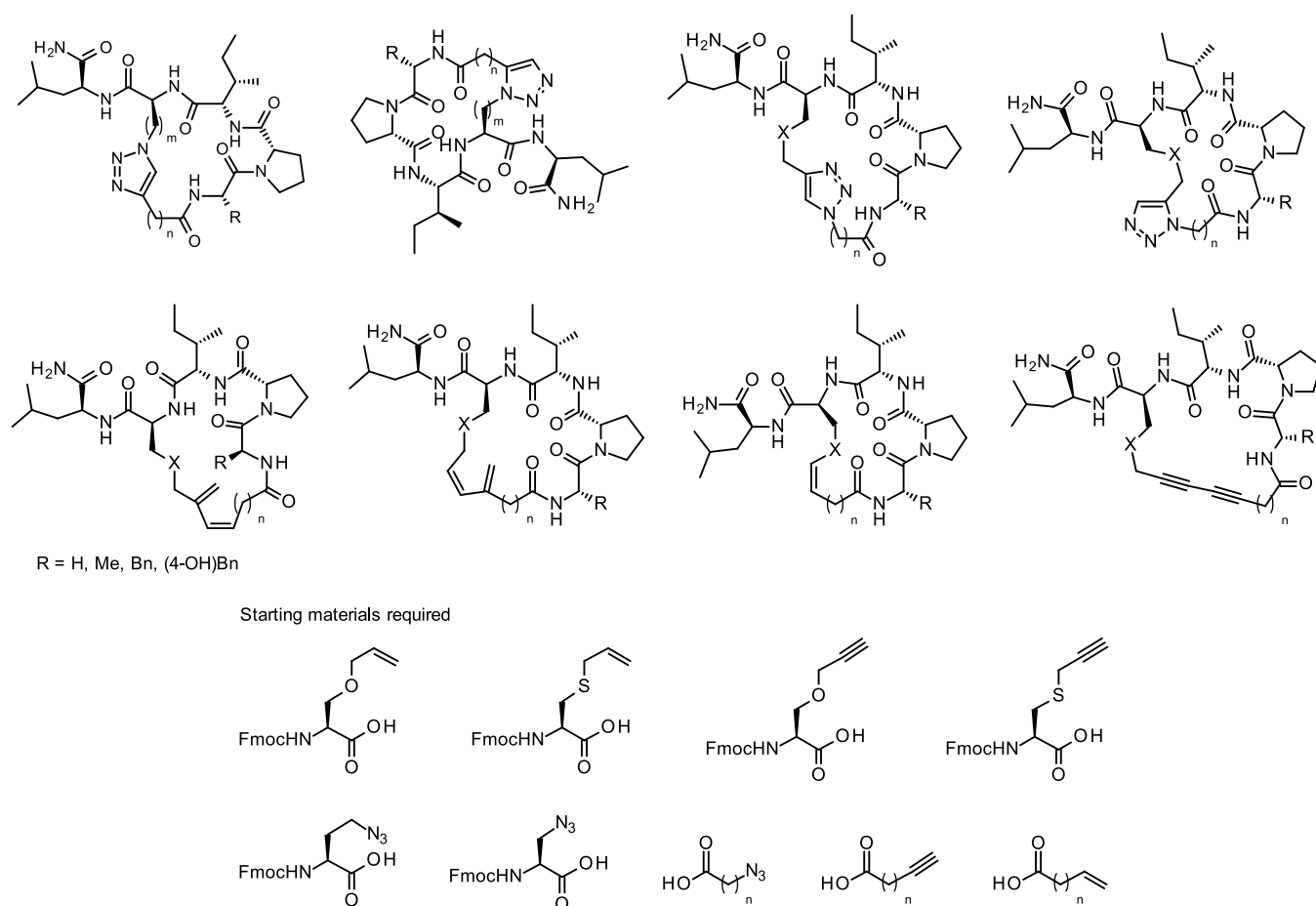
Figure 2. Stapled peptide structures, unnatural amino acids, and carboxylic acids required for their synthesis.

strategy for our approach. While peptide **1** and related 13-mer peptides demonstrate potent binding to KRAS in isolated protein assays (<50 nM IC$_{50}$), they show no cellular activity in antiproliferative or in ERK or AKT pathway inhibition assays when tested up to 10 μM (top concentration tested) in NCI-H358 and PC9 cells.[11] In this work, we sought to maintain the three key hydrophobic binding interactions with KRAS shown by the Takeda and AZ peptide inhibitors but with the aim to present these in simpler, more "drug-like", and membrane-permeable compounds. Our focus here was to identify a minimum peptide binding sequence and motif and use a stapling approach with high synthetic tractability to allow us to explore a wealth of different linkers and macrocyclization techniques with the aim of generating stapled-peptide libraries incorporating the key hydrophobic residues of the identified pharmacophore motif with a reasonable element of diversity.

CHEMISTRY

As described, we sought to apply learnings of the plethora of different stapling methodologies that have been developed.[17,18] These can be divided in two broad groups: one-component (1C) and two-component (2C) peptide stapling.[16] We chose to focus on the former where linking chemistry is used to directly tether two amino acid side chains. This generally requires the introduction of un-natural amino acids bearing suitable functional groups, but a few techniques rely on the use of nucleophilic side chains (cysteine, serine, and lysine).[19] Based on an assessment of the published work and building upon the previous experience of the Spring group,[20] we

identified the following cyclization techniques as viable options for quickly building a comprehensive library of stapled peptides: Cu-mediated and Ru-catalyzed azide−alkyne click chemistry (AACC) to yield 1,4- and 1,5-triazoles, respectively; ene−yne metathesis to yield 1,3-dienes; cross-alkene metathesis to yield alkenes; Glaser coupling to yield 1,3-diynes; Heck coupling to yield 1-arylethenes; and Sonogashira coupling to yield 1-arylethyne staples. In addition to the precedent for the cyclization chemistry, the potential to use common un-natural amino acids in a divergent approach to prepare multiple cyclized products and the synthesis of the required acyclic precursors by solid-phase peptide synthesis (SPPS) were important considerations in the initial library screening approach we adopted. We were also interested in employing the thiopropargyl linker present in compound **1**; however, synthesis of the amino acid used and incorporation in SPPS proved to be very challenging and intractable (see Supporting Information, Schemes S1 and S2), so this was not pursued further.

The structure of the peptides and nature of the cyclization chemistry of compounds initially prepared are outlined in Figure 2 and Table 1.

The linear precursor peptides were prepared using SPPS on a Rink Amide AM resin to obtain the C-terminal amide derivatives (Scheme 1). Deprotection of the Fmoc group to unveil the free amine was followed by coupling of the next Fmoc-protected amino acid in the presence of HATU and DIPEA (for manual synthesis), or EDC and ethyl cyanohydroxyiminoacetate (oxyma) (for peptide synthesizer syn-

Table 1. Linear Peptides, Macrocyclization Techniques, and Conditions[a]

R^2 = CH$_2$(4-OH-Ph), CH$_2$Ph, Me, H

X = O, S, CH$_2$

acyclic precursor		cyclic product	cyclization conditions
R^1	R^2	L	
			a (Cu-AACC)
			b (Ru-AACC)
			a (Cu-AACC)
			b (Ru-AACC)
			c (Glaser coupling)
			d (ene−yne metathesis)
			d (ene−yne metathesis)
			e (alkene cross-metathesis)
			f (Heck coupling)
			g (Sonogashira coupling)

[a]Macrocyclization reaction conditions: a, Cu-AACC: CuI, DIPEA, THF, reflux; b, Ru-AACC: [Cp*RuCl]4, THF, reflux; c, Glaser coupling: Cu(OAc)2, pyridine, DCM; d, ene−yne metathesis: Grubbs' II generation, ethylene, DCM, reflux; e, alkene cross-metathesis: Grubbs' II generation, DCM, reflux; f, Heck coupling: Pd(OAc)$_2$, K2CO3, MeCN, reflux; g, Sonogashira coupling: CuI, Pd(PPh$_3$)$_4$, HNEt$_2$, MeCN, reflux.

thesis). Cleavage of the peptide from the resin, using a mix of TFA/TIPS/H$_2$O 95:2.5:2.5, and purification *via* preparative HPLC yielded the desired compounds (Scheme 1).

Both *O*- and *S*-propargyl derivatives for ene−yne metathesis, Glaser coupling, and azide−alkyne click chemistry could be synthesized in good yields; synthesis of cross-alkene metathesis and Heck and Sonogashira coupling linear peptides proved

equally successful, with bromo-, iodo- and styrene-benzoic acids all successfully introduced into the linear sequences and purified in good yields (Table 2). Due to the ease of synthesis and to the fact that from a single linear peptide it would be possible to generate two entries in our library (1,4- and 1,5-triazole), azide−alkyne click chemistry precursors feature predominantly in the library. With these compounds in

Scheme 1. Synthesis of the Linear Peptides[a]
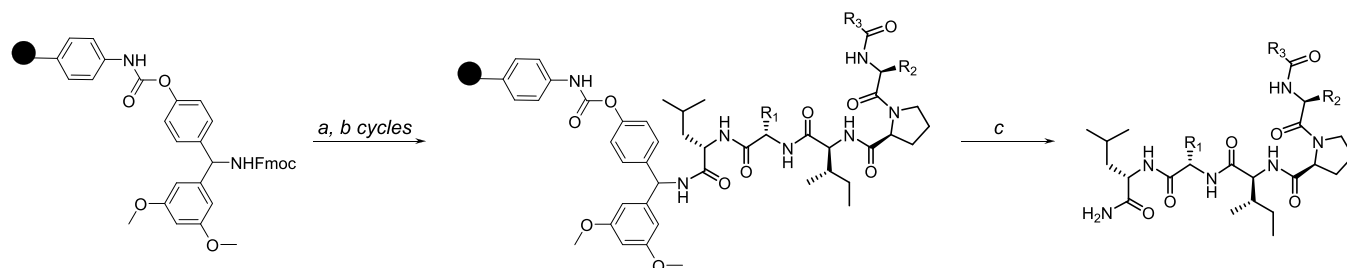
[a](a) Piperidine (20% v/v in DMF), 2 min; (b) HATU, amino acid, DMF, DIPEA, 3 min; (c) TFA/TIPS/H$_2$O 95:2.5:2.5, 1.5 h.

hand, we were able to prepare the macrocyclic peptides as indicated in Tables 1 and 2. The yields of cyclization chemistry were generally relatively modest but workable for isolation and *in vitro* biological testing. Some general differences in the relative efficiencies of the cyclization chemistries were observed. The Cu-AACC cyclization to 1,4-triazoles gave consistently higher yields than the Ru-AACC equivalent to prepare 1,5-triazoles. The ene−yne and cross-alkene metathesis reactions delivered -ene and -diene macrocycles in good yields. Cases where a phenyl ring was incorporated as the final capping acid component (2-vinyl and 3-vinyl benzoic acid) resulted in complex mixtures of products when subjected to the reaction conditions. Glaser coupling to deliver di-yne products also proved to be a more challenging macro-cyclization technique, only yielding three cyclized products from the nine linear adducts synthesized. We hypothesize that ring-strain of the di-yne products is the main barrier in this reaction being successful. In terms of Pd-catalyzed processes, all Sonogashira attempts only yielded the concurrently de-halogenated and de-propargylated linear adducts. Attempted Heck couplings behaved similarly with the exception of one compound (**21**). Overall, these methods allowed for the quick and effective buildup of a reasonable-sized library of compounds for initial screening.

The more detailed SAR exploration of binding residues that we then undertook followed the same principles where un-natural amino acids were introduced from their Fmoc derivatives by SPPS.

RESULTS AND DISCUSSION

In our initial investigations, in addition to exploring the impact of cyclization chemistry, we also investigated the necessity of the tyrosine residue. This amino acid is the only residue in the core peptides in our initial exploration that neither is providing a core hydrophobic binding group nor is a part of the staple cyclizing the peptide. Additionally, evidence from the crystal structure of **1** bound to KRAS indicated that this group was solvent exposed and not directly involved in binding. Guided by this general design approach, initial stapled peptides were synthesized and their KRAS binding potency was determined using a FRET-based competition assay. The key results of this work are detailed in Table 3.

It can be seen from these initial screen results that no compounds were identified with an IC$_{50}$ lower than 100 μM. However, we were able to compare the compounds on the basis of the inhibition at the highest tested concentration (100 μM), which allowed initial SAR conclusions to be made and provided direction for subsequent exploration. The Glaser coupling (**20**, **21**), cross-metathesis (**19**), and Heck coupling

(**22**) products proved to be completely inactive, whereas some inhibition could be observed in the products of the ene−yne metathesis (**16−18**) and azide−alkyne click chemistry (**1−15**). In the latter case, 1,5-triazole linkers gave higher levels of inhibition than 1,4-triazole linkers, and compounds derived with an oxygen link at residue 2 (prepared from *O*-propargyl serine derivatives) showed greater inhibition than analogues with a sulfur link (prepared from *S*-propargyl cysteine derivatives). The lack of critical importance of the tyrosine residue was demonstrated in this set of compounds, with Phe and Gly derivatives replacing the Tyr showing very similar binding potency (**7−10**). For simplicity, to reduce molecular weight, and for ease of synthesis, we quickly adopted Gly as the fifth residue in the synthesis of linear peptides. The size of the macrocycle ring did not show a significant trend in terms of inhibition. From this work, the compound showing the greatest inhibition was compound **10**, containing *O*-linked 1,5 triazole staple and glycine at residue 5. These structural features were adopted as standard for the subsequent exploration of other modifications. The activity of diene **18** was comparable to compound **10**, and its derivatives were also explored; however, results from this work were not favorable.

Having identified a simpler, synthetically accessible peptide with weak but measurable RAS binding, we next moved on to exploring and seeking to optimize the three hydrophobic residues that had been identified as providing the key interactions with the RAS protein. We first explored modification of the isoleucine position (residue 3; R^3 variation in Table 4). Modifications of the alkyl group at this position provided compounds with increased binding affinity. Substitution of isoleucine (**10**) for alanine (**23**) and cyclo-hexylalanine (**24**) resulted in no major loss or gain in activity, whereas increased activity, relative to the parent compound **10**, was observed when *nor*-leucine (**26**) or leucine (**25**) was introduced as residue 3. The latter variant is also present in the Takeda peptide.[8] The introduction of cyclopropylalanine (**27**) registered the highest activity observed with an alkyl side chain at this position; however, compounds with larger, more lipophilic aromatic residues further increased potency.

Moving from isoleucine to phenylalanine (**28**), to tryptophane (**31**), and to 3-(naphthyl)alanine (**32**, **33**) showed significant increases in potency, with the 1-naphthyl derivative **32** registering an IC$_{50}$ of 7.5 μM. It is worth noting that removing the methylene from the amino acid side chain, as when using phenylglycine (**29**), led to a complete loss of activity, indicating that its shape is not compatible with that of the binding pocket. Introduction of heteroatoms on the aryl ring, such as a nitrogen (pyridyl substituent, **34**) or a sulfur (thienyl substituent, **35**), or of chloro substituents (**36**, **37**) was not beneficial to potency, often leading to inactivity.

Table 2. Cyclic Peptide Preparation Details and Characterization

compd.	precursor linear peptide[a]	general cyclization procedure[b]	product yield (mg)	product yield (%)	HRMS calculated for	HRMS found	Δ (ppm)	retention time (HPLC)[c]
2	S1.1	A	6.45	44%	$C_{37}H_{56}O_7N_9S$: 770.4018	770.4003	−2	19.4 min
3	S1.2	A	4.4	48%	754.9 ($[M + H]^+$)			10.5 min
4	S1.3	A	4.3	43%	694.8 ($[M + H]^+$)			12.2 min
5	S1.4	A	4.27	33%	708.8 ($[M + H]^+$)			11.9 min
6	S1.1	B	4.2	46%	$C_{37}H_{55}O_7N_9SNa$: 792.3837	792.3814	−3	10.9 min
7	S1.2	B	3.91	42%	754.9 ($[M + H]^+$)			10.4 min
8	S1.5	B	1.87	11%	738.8 ($[M + H]^+$)			11.9 min
9	S1.6	B	2.22	13%	662.8 ($[M + H]^+$)			9.8 min
10	S1.7	B	0.59	3%	648.7 ($[M + H]^+$)			9.5 min
11	S1.8	B	0.5	3%	634.8 ($[M + H]^+$)			9.5 min
12	S1.9	A	2.19	17%	618.7 ($[M + H]^+$)			9.7 min
13	S1.10	B	1.39	15%	604.7 ($[M + H]^+$)			9.7 min
14	S1.11	B	2.09	11%	710.8 ($[M + H]^+$)			10.3 min
15	S1.9	B	1.45	11%	618.7 ($[M + H]^+$)			9.9 min
16	S1.12	D	3.16	23%	$C_{32}H_{52}N_6O_6S$: 649.3747	649.3771	3.7	13.2 min
17	S1.13	D	1.81	14%	$C_{30}H_{48}N_6O_7$: 605.3663	605.3644	3.1	12.5 min
18	S1.14	D	0.31	4%	591.8 ($[M + H]^+$)			11.5 min
19	S1.15	E	0.68	7%	$C_{30}H_{50}N_6O_7Na$: 629.3639	629.3661	3.5	12.9 min
20	S1.16	C	3.01	30%	$C_{32}H_{48}N_6O_7$: 629.3663	629.3661	0.3	12.5 min
21	S1.17	C	10.2	40%	$C_{31}H_{46}N_6O_7$: 615.3506	615.3528	3.6	11.4 min
22	S1.18	F	0.13	6%	627.7 ($[M + H]^+$)			15.9 min
23	S1.19	B	1.12	6%	$C_{27}H_{43}N_9O_7$: 606.3364	606.3369	0.8	10.8 min
24	S1.20	B	0.59	4%	$C_{33}H_{53}N_9O_7$: 688.4146	688.4142	0.6	12.2 min
25	S1.21	B	0.96	5%	$C_{30}H_{49}N_9O_7$: 648.3833	648.3863	4.6	11.4 min
26	S1.22	B	1.15	8%	$C_{30}H_{49}N_9O_7$: 648.3833	648.381	3.5	12.8 min
27	S1.23	B	0.1	1%	646.8 ($[M + H]^+$)			9.7 min
28	S1.24	B	0.2	3%	681.8 ($[M]^-$)			15.2 min
29	S1.25	B	0.96	16%	$C_{33}H_{47}N_9O_7$: 682.3677	682.3689	1.8	10.8 min
30	S1.26	B	0.48	8%	$C_{32}H_{45}N_9O_7$: 668.3520	668.351	1.5	11.2 min
31	S1.27	B	0.9	12%	$C_{35}H_{48}N_{10}O_7$: 721.3786	721.3755	4.3	10.9 min
32	S1.28	B	1.9	9%	$C_{37}H_{49}N_9O_7$: 732.3833	732.3807	3.6	12.4 min
33	S1.29	B	1.11	7%	$C_{37}H_{49}N_9O_7$: 732.3833	732.3862	4	12.5 min
34	S1.30	B	1.14	7%	683.7 ($[M + H]^+$)			10.7 min
35	S1.31	B	0.85	4%	$C_{31}H_{45}N_9O_7S$: 688.3241	688.3229	1.7	10.8 min
36	S1.32	B	0.92	5%	$C_{33}H_{46}N_9O_7Cl$: 716.3287	716.3315	3.9	13.8 min
37	S1.33	B	1.7	11%	$C_{33}H_{46}N_9O_7Cl$: 716.3287	716.3315	3.9	12.1 min
38	S1.34	B	4.53	47%	$C_{38}H_{51}N_9O_7$: 746.3990	746.3969	2.8	11.9 min
39	S1.35	B	1.15	7%	$C_{36}H_{47}N_9O_7$: 718.3677	718.3657	2.8	14.1 min
40	S1.36	B	0.33	3%	760.8 ($[M + H]^+$)			13.7 min
41	S1.37	B	1.67	9%	$C_{37}H_{49}N_9O_8$: 748.3782	748.378	0.3	11.3 min
42	S1.38	B	0.68	10%	$C_{37}H_{49}N_9O_8$: 748.3782	748.378	0.3	13.2 min
43	S1.39	B	0.85	8.50%	$C_{37}H_{49}N_9O_8$: 748.3782	748.378	0.3	11.5 min
44	S1.40	B	1.47	10%	$C_{37}H_{49}N_9O_8$: 748.3782	748.378	0.3	12.0 min
45	S1.41	B	0.35	8%	$C_{38}H_{53}N_9O_7$: 748.4146	748.4172	3.5	13.0 min
46	S1.42	B	3.5	24%	$C_{36}H_{49}N_9O_7$: 720.3833	720.3807	3.6	12.5 min
47	S1.43	B	0.84	6%	$C_{42}H_{51}N_9O_7$: 794.3990	794.398	1.3	14.1 min
48	S1.44	B	2.04	7%	$C_{34}H_{43}N_9O_7$: 690.3364	690.333	4.9	11.0 min
49	S1.45	B	1.29	13%	$C_{39}H_{51}N_9O_7$: 758.3990	758.3964	3.4	13.1 min
50	S1.46	B	0.7	5%	$C_{40}H_{53}N_9O_7$: 772.4146	772.4135	1.4	13.9 min
51	S1.47	B	0.5	4%	$C_{37}H_{49}N_9O_7$: 732.3833	732.3862	4	12.6 min
52	S1.48	B	1.21	8%	$C_{37}H_{47}N_9O_7$: 730.3677	730.3655	3	12.7 min
53	S1.49	B	0.98	5%	$C_{35}H_{44}N_{10}O_8$: 733.3422	733.345	3.8	10.2 min
54	S1.50	B	0.45	3%	747.8 ($[M + H]^+$)			10.2 min
55	S1.51	B	0.77	9%	$C_{38}H_{51}N_9O_7$: 746.3990	746.4025	4.7	12.7 min
56	S1.52	B	2.2	12%	$C_{38}H_{51}N_9O_7$: 746.3990	746.4025	4.7	12.4 min
57	S1.53	B	1.26	9%	$C_{38}H_{51}N_9O_7$: 746.3990	746.4025	4.7	12.5 min
58	S1.54	B	1	5%	$C_{39}H_{51}N_9O_9$: 790.3888	790.3873	1.9	12.3 min
59	S1.55	B	0.33	3%	804.7 ($[M + H]^+$)			11.8 min

Table 2. continued

compd.	precursor linear peptide[a]	general cyclization procedure[b]	product yield (mg)	(%)	HRMS calculated for	found	Δ (ppm)	retention time (HPLC)[c]
60	S1.56	B	0.21	2%	788.8 ([M − H]−)			12.6 min
61	S1.57	B	0.19	2%	804.7 ([M + H]+)			12.8 min
62	S1.58	B	3.53	13%	$C_{34}H_{43}N_9O_7$: 690.3364	690.3384	2.9	12.2 min
63	S1.59	B	2.47	14%	$C_{35}H_{45}N_9O_7$: 704.3520	704.3502	2.6	12.3 min
64	S1.60	B	2.72	11%	$C_{36}H_{47}N_9O_7$: 718.3677	718.3657	2.8	12.4 min
65	S1.61	B	1.86	11%	$C_{35}H_{46}N_8O_6$: 675.3619	675.3604	2.2	12.8 min
66	S1.62	B	2.02	8%	$C_{36}H_{48}N_8O_6$: 689.3775	689.376	2.2	13.3 min
67	S1.63	B	0.87	6%	$C_{38}H_{52}N_8O_6$: 717.4088	717.4113	3.5	14.7 min
68	S1.64	B	1.57	10%	$C_{40}H_{56}N_8O_6$: 745.4401	745.4408	0.9	16.3 min
69	S1.65	B	1.25	6%	$C_{37}H_{49}N_9O_6S$: 748.3605	748.3612	0.9	15.1 min
70	S1.66	B	2.7	16%	$C_{38}H_{51}N_9O_6$: 730.4041	730.4042	0.1	12.2 min
71	S1.67	B	2.55	8%	$C_{36}H_{47}N_9O_6$: 702.3728	702.374	1.7	12.7 min
72	S1.68	B	2.08	9%	$C_{35}H_{45}N_9O_6$: 688.3571	688.3551	2.9	12.9 min
73	S1.69	B	3.51	14%	$C_{36}H_{47}N_9O_6$: 702.3728	702.374	1.7	14.4 min
74	S1.28	A	7.68	33%	732.3 ([M + H]+)			12.2 min
75	S1.70	B	0.5	6%	900.7 ([M + H]+)			
76	S1.71	B	1.2	7%	$C_{43}H_{57}N_{11}O_{11}$: 904.4317	904.4336	2.1	11.6 min
77	S1.72	B	1.3	11%	$C_{44}H_{59}N_{11}O_{11}$: 918.4474	918.4493	2.1	11.5 min
78	S1.73	B	4.5	19%	$C_{51}H_{69}N_{13}O_{13}$: 1072.5216	1072.523	0.9	11.2 min
79	S1.74	B	2.2	15%	$C_{52}H_{71}N_{13}O_{13}$: 1086.5373	1086.539	1.1	11.4 min
80	S1.75	B	1.9	9%	$C_{54}H_{81}N_{13}O_{14}$: 1136.6104	1136.615	3.7	12.6 min
81	S1.76	B2	0.99	10%	1829.8 ([M + H]+)			12.5 min
82	S1.77	B2	1.36	14%	1912.6 ([M + H]+)			13.5 min

[a]Starting linear peptides; see Table S1 in the Supporting Information. [b]Procedure details in the Experimental Section: Chemistry. Procedure labels (capitals) correspond to reaction condition labels in Table 1 (lower case). [c]HPLC conditions in the Experimental Section: Chemistry.

We then moved forward into exploring the other features of our structures using compound **32** as the new start point for further modifications, starting with variation of the proline (residue 4, Table 4). Expansion of the proline ring to the six-membered homo-proline resulted in little change in activity (**38**); this SAR was confirmed for other proline/homo-proline pairs (data not included). In contrast to the generally neutral impact on potency in going from proline to homoproline, contraction of the proline pyrrolidine ring to an azetidine resulted in a significant loss of activity (**39**). We envisioned that further expansion to a seven-membered ring could prove beneficial, so we synthesized azepane-2(S)-carboxylic acid following literature precedent.[21] However, the resulting stapled peptide showed reduced activity in comparison to the five- and six-membered ring analogues (**40**). Consistent with its interaction with a hydrophobic binding pocket, introduction of hydroxyl groups on the proline ring at the 3- and 4-position resulted in loss of potency (**41−43**). Interestingly, replacement of the piperidine ring of the homo-proline with a morpholine ring resulted in retention of potency (**44**). In contrast, "opening" the proline ring by introduction of N-methyl valine in place of proline resulted in complete loss of activity (**45**), whereas introduction of gem-dimethyl glycine yielded a compound (**46**) only 3-fold less potent than the standard **32**. This likely reflects the role of the proline in the conformation of the macrocyclic peptide as well as its hydrophobic interaction. It is of note that introduction of a larger group such as iso-quinoline (**47**) resulted in potency being maintained. While this does not reflect the potential increased potency from a larger hydrophobic interaction, it does seem to indicate some flexibility in the nature of the binding pocket such that any detrimental change due to the

adapted binding mode resulting from the introduction of this much larger group is able to be compensated. However, it is also interesting to note that this accommodation is not always possible given the loss of potency shown by the seven-membered ring derivative **40**.

We next explored modification of the third key hydrophobic residue, the leucine residue 1 (Table 4). A range of nonpolar alkyl substituents was explored and resulted in loss of binding affinity, suggesting that affinity is sensitive to small changes at this position (**48−52**). It is striking that the simple substitution of a leucine (**32**) for a nor-leucine (**51**) resulted in a 13-fold loss of activity. It would seem that the flexibility of this hydrophobic pocket is limited and that optimal hydrophobic interactions are relatively specific. Possibly consistent with this finding, examination of the binding site in the original crystal structure suggested the possibility that more hydrophilic interactions could also occur. To explore the potential benefit from polar hydrogen bonding interactions that could be accessed by residue 1 on the peptide, the introduction of polar side chains of an asparagine or a glutamine residue was made (**53, 54**). While a significant loss in potency resulted, this was less than with some alkyl side chains, indicating some subtlety in the binding interactions at this site.

As part of a broader exploration, we sought to introduce N-methyl derivatives sequentially at all residues; however, due to synthetic difficulties and limitations either in the synthesis of the required amino acid or in the efficiency of coupling within the peptide sequence, the introduction of N-methyl leucine instead of leucine at residue 1 was the only residue where this was achieved. This change resulted in a loss of binding potency (**55**), possibly indicating a role of this backbone NH in

Table 3. Selected Examples of Macrocycles with RAS Binding Activity

stapled peptide	L	m	n	X	R	RAS binding assay IC$_{50}$ (μM)[a]	inhibition at 100 μM
1						0.023	
2	A	1	4	SCH$_2$	CH$_2$(4-OH-Ph)	>100	0%
3	A	1	4	OCH$_2$	CH$_2$(4-OH-Ph)	>100	22%
4	C	1	3		CH$_2$Ph	>100	8%
5	C	2	3		CH$_2$Ph	>100	9%
6	B	1	4	SCH$_2$	CH$_2$(4-OH-Ph)	>100	20%
7	B	1	4	OCH$_2$	CH$_2$(4-OH-Ph)	>100	28%
8	B	1	4	OCH$_2$	CH$_2$Ph	>100	38%
9	B	1	4	OCH$_2$	Me	>100	30%
10	B	1	4	OCH$_2$	H	100	48%
11	B	1	3	OCH$_2$	H	>100	39%
12	C	2	3		H	>100	6%
13	D	1	3		H	>100	16%
14	D	2	2		CH$_2$(4-OH-Ph)	>100	44%
15	D	2	3		H	>100	22%
16	F	1	3	SCH$_2$	Me	>100	28%
17	G	1	2	OCH$_2$	H	>100	21%
18	G	1	1	OCH$_2$	H	98	46%
19	I	1	3	OCH$_2$	Me	>100	5%
20	E	1	3	OCH$_2$	Me	>100	0%
21	E	1	3	OCH$_2$	H	>100	0%
22	H	1	0	OCH$_2$	Me	>100	25%

[a]Reported IC$_{50}$ values are the geometric means of independent IC$_{50}$ measurements of a 12-point concentration–response curve with a maximum concentration of 100 μM.

hydrogen bonding or a significant conformational change induced by methylation.

Having explored variation of the ligand structure at the three key sites of interaction initially identified and found compounds with micromolar binding potency, we sought to confirm that the more potent compounds retained the expected binding interactions. We attempted co-crystallization of compounds (**32**, **38**) with the KRAS^{G12V} construct to generate crystals from the X-ray structure determination. Unfortunately, all attempts failed to deliver crystals with ligand bound. We concluded that limitations in the peptides' potency and/or solubility in the crystallization media were the likely cause of this failure.

We then sought to find and explore alternative sites and approaches where additional gains in potency could be found. First, we turned to modification of the glycine position, residue 5 (Table 5), to explore whether beneficial conformational restriction could be found. Introduction of a methyl group with both L- and D-alanine resulted in a relatively minor reduction of activity, more so when using the non-natural D-enantiomer (**56**, **57**). The introduction of a side chain at that position can provide a strong conformational bias, and the absolute stereochemistry of the position would have an additional influence on the shape. The relatively similar potency of these compounds appears to indicate the lack of a strong conformational requirement at this position and supports the

earlier conclusion of no significant binding interaction from the side chain. For an additional exploration at this position, we sought to introduce an acidic residue in an attempt to mimic the aspartate residue in the Takeda peptide KRpep-2d. The reported alanine scan of this peptide highlighted the importance of a residue (Asp12), whereupon D12A modification led to a 1000-fold loss in potency, an unexpected result for a solvent-exposed residue.[8] Based on the crystal structure analysis, Sogabe et al. proposed that residue held such importance due to the formation of a salt bridge with one of the solvent-exposed Arg102 of KRAS.[8] We reasoned that we could try to introduce a similar interaction to increase the potency of our peptides. While there was no obvious direct equivalent for the introduction of such an acidic residue, we reasoned, based on our expected binding mode, that substituting the glycine residue (residue 5) with acidic amino acids could deliver an equivalent interaction to that seen by Asp12 in the Takeda peptide.[8b] To fully explore this possibility, we prepared L- and D-stereoisomers of both aspartate and glutamate (**58**–**61**). Unfortunately, this did not prove to be beneficial as these modifications led to a loss in potency, especially when using the un-natural D-amino acids (**60**, **61**).

We then moved forward to a more detailed exploration of the size of the macrocycle and the nature of the linking triazole (Table 5). We hypothesized that such changes could alter the

Table 4. SAR of Side Chain Changes of Residues 3, 4, and 1

| compd.	R^1	R^2	R^3	R^4	R^5	RAS binding assay		
						mean IC$_{50}$ (μM)	n^a	pIC$_{50}$ ± SE
10	CH$_2$i-Pr	H	(S)-CH-[(S)-Me]-Et	H	A	100	2	4
23	CH$_2$i-Pr	H	(S)-Me	H	A	91	3	4.04 ± 0.04
24	CH$_2$i-Pr	H	(S)-CH$_2$(cyclohexyl)	H	A	100	2	4.0 ± 0.0
25	CH$_2$i-Pr	H	(S)-CH$_2$i-Pr	H	A	60	3	4.22 ± 0.05
26	CH$_2$i-Pr	H	(S)-n-Bu	H	A	48	4	4.32 ± 0.16
27	CH$_2$i-Pr	H	(S)-CH$_2$(cyclopropyl)	H	A	32	1	4.49
28	CH$_2$i-Pr	H	(S)-CH$_2$Ph	H	A	>38	7	<4.4 ± 0.14
29	CH$_2$i-Pr	H	(R)-CH$_2$Ph	H	A	>82	5	<4.1 ± 0.04
30	CH$_2$i-Pr	H	(S)-Ph	H	A	>100	2	<4
31	CH$_2$i-Pr	H	(S)-CH$_2$(3-indolyl)	H	A	18	3	4.74 ± 0.06
32	CH$_2$i-Pr	H	(S)-CH$_2$(1-naphthyl)	H	A	7.1	3	5.15 ± 0.12
33	CH$_2$i-Pr	H	(S)-CH$_2$(2-naphthyl)	H	A	9.5	3	5.02 ± 0.07
34	CH$_2$i-Pr	H	(S)-CH$_2$(3-pyridyl)	H	A	41	1	4.39
35	CH$_2$i-Pr	H	(S)-CH$_2$(3-thienyl)	H	A	53	3	4.27 ± 0.08
36	CH$_2$i-Pr	H	(S)-CH$_2$(2-Cl-Ph)	H	A	>100	2	<4
37	CH$_2$i-Pr	H	(S)-CH$_2$(4-Cl-Ph)	H	A	>74	6	<4.1 ± 0.08
38	CH$_2$i-Pr	H	(S)-CH$_2$(1-naphthyl)	H	B	7.7	3	5.12 ± 0.12
39	CH$_2$i-Pr	H	(S)-CH$_2$(1-naphthyl)	H	C	32	3	4.49 ± 0.07
40	CH$_2$i-Pr	H	(S)-CH$_2$(1-naphthyl)	H	D	55	2	4.26 ± 0.05
41	CH$_2$i-Pr	H	(S)-CH$_2$(1-naphthyl)	H	E	38	3	4.42 ± 0.05
42	CH$_2$i-Pr	H	(S)-CH$_2$(1-naphthyl)	H	F	95	3	4.02 ± 0.01
43	CH$_2$i-Pr	H	(S)-CH$_2$(1-naphthyl)	H	G	70	3	4.16 ± 0.07
44	CH$_2$i-Pr	H	(S)-CH$_2$(1-naphthyl)	H	H	6.5	4	5.19 ± 0.11
45	CH$_2$i-Pr	H	(S)-CH$_2$(1-naphthyl)	H	I	100	2	4.0 ± 0.0
46	CH$_2$i-Pr	H	(S)-CH$_2$(1-naphthyl)	Me	J	20	3	4.71 ± 0.09
47	CH$_2$i-Pr	H	(S)-CH$_2$(1-naphthyl)	H	K	5.8	3	5.24 ± 0.03
48	Me	H	(S)-CH$_2$(1-naphthyl)	H	A	37	4	4.43 ± 0.17
49	c-hexyl	H	(S)-CH$_2$(1-naphthyl)	H	A	78	3	4.11 ± 0.12
50	CH$_2$c-hexyl	H	(S)-CH$_2$(1-naphthyl)	H	A	100	1	4
51	n-Bu	H	(S)-CH$_2$(1-naphthyl)	H	A	100	1	4
52	CH$_2$c-propyl	H	(S)-CH$_2$(1-naphthyl)	H	A	29	4	4.54 ± 0.18
53	CH$_2$CONH$_2$	H	(S)-CH$_2$(1-naphthyl)	H	A	48	4	4.31 ± 0.12
54	CH$_2$CH$_2$CONH$_2$	H	(S)-CH$_2$(1-naphthyl)	H	A	50	2	4.30 ± 0.0
55	CH$_2$i-Pr	Me	(S)-CH$_2$(1-naphthyl)	H	A	26	2	4.59 ± 0.14

^{a}Number of independent assay replicates.

conformational bias within the macrocycle and could lead to the optimal presentation of the key hydrophobic residues. Shortening the azido-bearing chain while retaining the glycine amino acid resulted in effective retention of potency for all the 2-, 3- and 4-carbon linkers (62−64), supporting the initial SAR gathered; more striking is the fact that exclusion of the glycine from the peptide sequence results in a substantial loss of activity even when ring-size is retained (65−68). In terms of the length and nature of the linking chain on the second amino acid, substitution of the oxygen for a sulfur did not significantly affect the activity, while substitution with a methylene group resulted in a 3-fold loss in potency (69, 70). Reduction of the length of the linker to one carbon unit was also detrimental to the activity of the peptide (71). Inverting the position of the azide and the alkyne moieties, i.e., generating isomeric 1,5-triazoles in the cyclized product, resulted in little change in activity (72, 73). We checked that the 1,4-triazole equivalent 74 of the most potent 1,5-triazole 32 was inactive, thus confirming the initial SAR data and choice of linker strategy. These results of exploration of changes in linker length and chemistry would appear to indicate that the 1,5-triazole provides no specific interactions, but the conformational effect of having the 1,5-triazole is important to drive more potent

activity. The inclusion of the glycine increases potency, but the impact of changes in overall ring size is less clear.

In light of the extensive library synthesized and the SAR conclusions drawn, and the failure to achieve sub-micromolar potencies, we decided to embark upon extending peptide 32 with equivalent residues from the original 14-mer peptide 1 (Table 6). We reasoned that our initial hypothesis that a shortened sequence could be optimized to deliver the three key binding residues may have been incorrect or at least insufficient. By "reintroduction" of residues present in peptide 1, we aimed to increase the potency of the macrocycle by either picking up further interactions on the protein surface or effecting a positive impact on the conformation of the macrocycle and presentation of the key hydrophobic groups. We decided to start by extending the peptide singularly in each direction, thus adding an Ala-Pro at the C-terminus, or an aspartate or a glutamate at the N-terminus (75−77). The elongation at the C-terminus and the Asp addition at the N-terminus resulted in a 5-fold loss of potency, whereas the addition of the glutamate registered an IC$_{50}$ closer to 100 μM. We reasoned that combining the two modifications might result in improved potency, so we synthesized extended parent compounds bearing both C- and N-terminus extensions, as

Table 5. SAR of Side Chain Changes of Residue 5, the Size of the Macrocycle, and Exclusion of Glycine
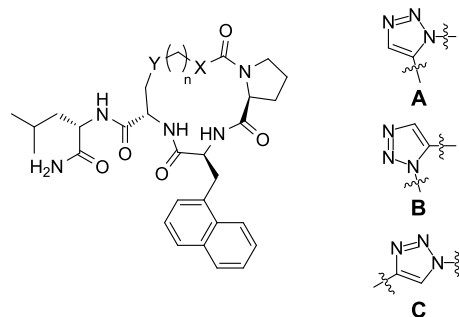
compd.	Y	X	R	n	RAS binding assay		
					mean IC$_{50}$ (μM)	n^a	pIC$_{50}$ ± SE
32	OCH$_2$-**A**	CONHCHR	H	4	7.1	3	5.15 ± 0.12
56	OCH$_2$-**A**	CONHCHR	(S)-Me	4	9.7	3	5.01 ± 0.1
57	OCH$_2$-**A**	CONHCHR	(R)-Me	4	25	3	4.6 ± 0.09
58	OCH$_2$-**A**	CONHCHR	(S)-CH$_2$CO$_2$H	4	66	3	4.18 ± 0.1
59	OCH$_2$-**A**	CONHCHR	(S)-CH$_2$CH$_2$CO$_2$H	4	49	2	4.31 ± 0.01
60	OCH$_2$-**A**	CONHCHR	(R)-CH$_2$CO$_2$H	4	77	1	4.11
61	OCH$_2$-**A**	CONHCHR	(R)-CH$_2$CH$_2$CO$_2$H	4	100	1	4
62	OCH$_2$-**A**	CONHCHR	H	1	9.6	7	5.02 ± 0.11
63	OCH$_2$-**A**	CONHCHR	H	2	7	3	5.15 ± 0.07
64	OCH$_2$-**A**	CONHCHR	H	3	10	3	4.98 ± 0.05
65	OCH$_2$-**A**			4	48	3	4.32 ± 0.04
66	OCH$_2$-**A**			5	12	4	4.90 ± 0.15
67	OCH$_2$-**A**			7	81	3	4.09 ± 0.09
68	OCH$_2$-**A**			9	28	5	4.55 ± 0.08
69	SCH$_2$-**A**	CONHCHR	H	4	11	3	4.98 ± 0.06
70	(CH$_2$)$_2$-**A**	CONHCHR	H	4	19	3	4.71 ± 0.04
71	**A**	CONHCHR	H	4	65	3	4.19 ± 0.12
72	**B**	CONHCHR	H	3	31	3	4.50 ± 0.03
73	CH$_2$-**B**	CONHCHR	H	3	13	3	4.90 ± 0.02
74	OCH$_2$-**C**	CONHCHR	H	4	>100	2	<4

^{a}Number of independent assay replicates.

Table 6. SAR upon Extension of the Peptide
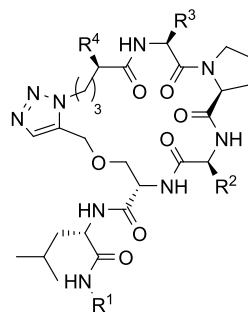
compound	R^1	R^2	R^3	R^4	RAS binding assay		
					mean IC$_{50}$ (μM)	n^a	pIC$_{50}$ ± SE
32	H	CH$_2$(1-naphthyl)	H	H	7.1	3	5.15 ± 0.12
75	Pro-Ala	CH$_2$(1-naphthyl)	H	H	46	5	4.34 ± 0.14
76	H	CH$_2$(1-naphthyl)	H	Asp-Ac	38	5	4.42 ± 0.06
77	H	CH$_2$(1-naphthyl)	H	Glu-Ac	93	5	4.03 ± 0.03
78	Pro-Ala	CH$_2$(1-naphthyl)	H	Asp-Ac	40	5	4.40 ± 0.06
79	Pro-Ala	CH$_2$(1-naphthyl)	H	Glu-Ac	>83	5	<4.1 ± 0.05
80	Pro-Leu	CH-[(S)-Me]-Et	CH$_2$(4-OH-Ph)	Asp-Ac	>89	4	<4.1 ± 0.05
81	Pro-Pro-Leu	CH-[(S)-Me]-Et	CH$_2$(4-OH-Ph)	Asp-Tyr-Phe-His-Phe-Ac	8.6	3	5.07 ± 0.13
82	Pro-Pro-Leu	CH$_2$(1-naphthyl)	CH$_2$(4-OH-Ph)	Asp-Tyr-Phe-His-Phe-Ac	3.3	3	5.48 ± 0.09

^{a}Number of independent assay replicates

well as both Asp and Glu (**78**, **79**); furthermore, we decided to use Leu instead of Ala at the C-terminus so as to reproduce the sequence reported in **1** (**80**). However, all these peptides registered potencies lower than the single-modification compounds, and the adduct bearing the original sequence **80** showed a potency 2-fold reduced in respect to Ala-bearing peptide **78**. To fully confirm that the truncated peptide does not result in detrimental interactions with the protein or suffer from intramolecular interactions that would enforce an unfavorable conformation, we decided to synthesize the equivalent 14-mer peptide with the 1,5-triazole linker. Derivatives **81** and **82**, respectively bearing an Ile and a 3-(1-naphthyl)alanine as the third residue, were made. It was interesting to note that these compounds showed increased potency when compared to the partially truncated peptides, but their potency was still comparable with the most potent cases obtained from the smaller 6-mer macrocycles of our library.

Having found compounds that were active in a simple RAS binding assay, we sought to confirm that these compounds inhibited RAS functional activity. The original larger peptides that were active in the binding assay were also active in inhibiting KRAS nucleotide exchange in a cell-free assay. We therefore sought to confirm that this was also the case for the smaller stapled peptides that we report here. Selected compounds were tested in a RAS/RAF nucleotide exchange assay (Table 7).[22] The data generated are consistent with

Table 7. Confirmation of Activity by Inhibition of KRAS Nucleotide Exchange

compound	RAS binding assay IC$_{50}$ (μM)	RAS/RAF nucleotide exchange assay IC$_{50}$ (μM)[a]
2	>100	>30
3	>100	>30
4	>100	>30
5	>100	>30
6	>100	>30
7	>100	>30
32	7.1 ± 2.3	2.4
38	7.7 ± 2.5	2.4
44	6.5 ± 1.9	5.0
62	9.6 ± 2.8	3.2
63	7.0 ± 1.2	3.6
64	10 ± 1.2	4.1
69	11 ± 1.6	2.5

[a]Single measurements.

expectations and demonstrate that these compounds act as functional inhibitors of RAS with comparable potencies to those observed in the RAS binding assay.

Finally, in regard to biological testing, two of the more potent compounds found in this work, **32** and **38**, were tested for antiproliferative activity in a 3D soft agar cellular proliferation assay. Both compounds showed inhibition of the proliferation of NCI-H358 and PC9 cells but only at the top concentration tested of 50 μM. While we cannot be certain if this activity can be attributed to the RAS inhibitory activity of these compounds or consider this a confirmation of cellular membrane permeability, it is of some encouragement that the drop-off from binding to cellular potency appears to be lower than the original 14-mer and 13-mer peptides that were the starting point for this work. Yet, it is clear that more potent

inhibitors would be required to more meaningfully explore potential cell activity.

While the confirmed biochemical activity and the SAR generated confirmed the general approach taken, the potency levels of the best truncated compounds identified remained relatively modest. Even for the most potent compounds, potencies were still approximately 100-fold lower than the original starting peptide **1** or peptide KRpep-2d reported by the Takeda group. In an attempt to direct efforts toward more potent derivatives, we sought to better understand and rationalize the factors limiting the potency of the compounds prepared. There are several possible reasons for the limited potency seen, but there would seem to be two main possibilities: one is that the simple pharmacophore of three hydrophobic residues interacting with RAS is insufficient to give peptides with the highest activity; i.e., there are other critical interaction(s), such as between a surface arginine of KRAS and Asp10 in peptide **1**. This is spatially similarly to Asp12 of KRpep-2d, which was found to make an important contribution to the potency of the Takeda peptide.[8] The other main possibility is that the peptides we have prepared do not favorably present the key residues for optimal binding with RAS. The data generated with the fuller-length peptides, **81** and **82**, would appear not to support the former explanation, or at least if additional interactions to the hydrophobic triad were key, then the conformation of the macrocycle in these compounds prevented these additional positive interactions from being evident in **81** and **82**. Thus, it would appear likely that the conformational bias of the macrocycle is key to the potencies seen whether the three hydrophobic interactions are sufficient for potent binding or not. To explore this, we tried to better understand the conformational preferences of the macrocyclic peptides prepared in this work. Specifically, we investigated the preferred conformations of the weakly active 1,4- and 1,5-triazole peptides **12** and **15** in the solution by NMR as prototypical examples.

The NMR analysis of macrocycle **12** (see Tables S3 and S4 and Figure S2 in the Supporting Information) suggests that a preferred conformer exists in the solution with well-defined resonances and with a significant degree of rigidity. The ^{1}H NMR signals of methylene groups within the macrocyclic ring appear split in the spectra,[23] indicating that different chemical environments exist on the NMR time scale. Furthermore, the triazole shows a preferred conformation in the solution with the aromatic proton pointing toward the core of the macrocycle, as indicated by long-range NOEs. An additional indication of rigidity comes from the $^3J_{\text{NH-H}\alpha}$ values of 8.7 and 9.3 Hz found for the two nonglycine amides in the ring, both deviating significantly from the 7.5 Hz mean value normally interpreted as arising from free mobility.[24] No strong intramolecular hydrogen bonds were found upon exchanging the solvent to 100% D$_2$O. Combining the NMR restraints (NOEs and J couplings) with molecular dynamics (MD) simulations in water, we determined the conformer that shows the highest agreement with the experimental data (Figure 3a–c). This conformer was aligned with the conformation of the peptide **1** found in the protein crystal structure with KRAS[11] from which we concluded that the solution conformer of **12** aligns reasonably well with the binding mode of peptide **1** (Figure 3d). However, further inspection suggested that clashes with the protein could arise from this binding mode.

In contrast, the equivalent 1,5-triazole, **15**, shows higher flexibility features than shown by **12**, with no splitting of the
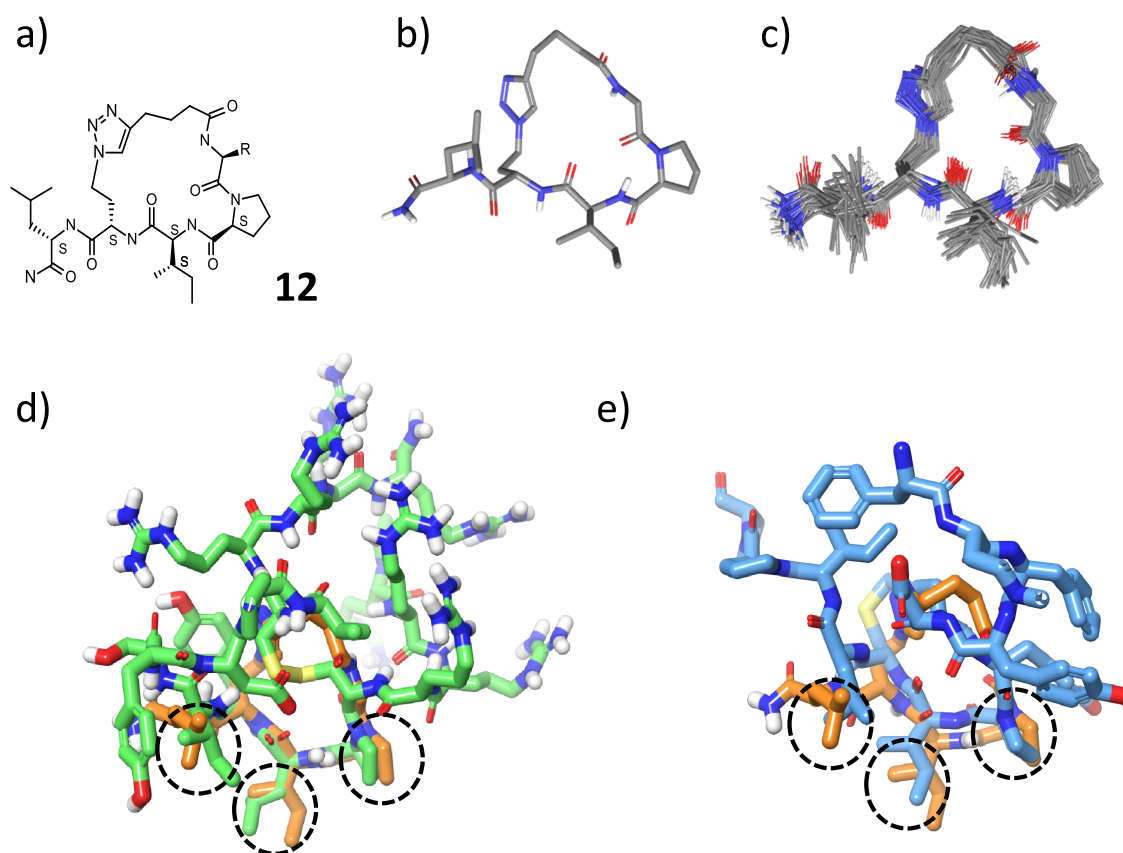
Figure 3. (a) Structure of peptide **12**. (b) Representation of the average solution conformation of compound **12**. (c) Conformational cluster from the unrestrained 10 ns MD simulation in the solvent that fits best with the experimental NMR data. (d) Solution conformation of **12** (orange) aligned with the KRpep-2d peptide (shown in green). The KR-pep-2d structure (Sogabe et al.[8]) was extracted from PDB entry 5XCO. (e) Solution conformation of **12** (orange) aligned with the conformation of peptide **1** (blue) from the protein crystal structure with KRAS. The three-point hydrophobic pharmacophore is indicated by dotted circles.

CH$_2$ groups in the NMR and $^3J_{NH\text{-}H\alpha}$ couplings in the range 7.3−7.5 Hz (free mobility). Additionally, no long-range NOEs were observed, and no intramolecular H-bonds were detected. Therefore, we concluded that this molecule does not show a preferred conformation in the solution. Next, we analyzed compound **38**, one of the more active 1,5-triazoles. This showed similar features to **15** with flexible conformational features, no indication of a preferred conformation, and no internal hydrogen bonds.

We further applied NMR analyses to explore whether apparent conformational differences could be shown to explain occurrences of surprising SAR, for example, that shown by the 2-chlorophenylalanine derivative **36**, which showed poor RAS binding potency with an IC$_{50}$ greater than 100 μM, while the corresponding phenylalanine analogue **28** showed at least 5-fold greater potency. However, similar features were found for **36** as seen for other 1,5-triazoles; that is, they demonstrate conformational flexibility, show no internal hydrogen bonds, and do not have a preferred conformation in the solution. Thus, while it would still seem most plausible that conformational differences are likely to explain the changes in activity between pair **28** and **36**, a clear evidence of such conformational effects is not present in the NMR analyses performed.

To check whether conformational effects might be evident across the wider library, we looked at measured physicochemical properties and equivalent calculated properties derived from the compounds' 2D structures. We measured polarity using an experimental chromatographic polar surface area

(ePSA) assay and compared this to the calculated PSA to gauge whether there were anomalies there that could indicate conformational influence. While the ePSA values were significantly lower than the calculated PSA, the library of stapled peptides demonstrated a consistent difference between these two values (data not shown). A similar conclusion was evident from the comparison of measured logD and calculated logP values. We conclude that this lack of significant difference between the relative behavior of different macrocyclic subclasses in terms of PSA and lipophilicity is consistent with the general lack of significant internal hydrogen bonding and would indicate the absence of any particularly preferred conformations between compounds and subclasses that showed differential presentation, or shielding, of polar residues.

While our conformational analysis shows differences in behavior between the more potent 1,5-triazole compounds and their less potent 1,4-triazole analogues, it does not give a clear understanding of the factors behind their relative potency difference or the potency difference to peptide **1**. However, it should be considered that, though compound **12** shows a preferred conformation in D$_2$O that would appear to fit the pocket reasonably well, this is not necessarily the same as the structure bound to KRAS. Additionally, the lack of a preferred solution conformation shown by the more potent 1,5-triazole compounds would further indicate that the preferred solution conformation of **12** is not optimal for binding. Finally, to investigate potential drivers of binding potency further, we employed molecular dynamics to establish whether the binding

mode of **12** is stable and persists. MD results suggest that the hydrophobic interaction patterns of peptide **12** and a truncated version of peptide **1** are comparable and that their core binding modes are stable over the course of a 100 ns MD run. Another outcome of the simulation of a truncated version of peptide **1** is to indicate that the interaction of Asp10 of peptide **1** and Arg102 of KRAS is favorable, but this interaction was not as stable as the hydrophobic interactions in the MD run (see Figures S4–S7 in the Supporting Information). These simulations do not clearly explain what limits the potency of the compounds identified in this work, but it could suggest that overall shape and charge complementarity to the protein and conformational stability are less good than those of the larger peptide **1**.

CONCLUSIONS

In conclusion, starting from a pharmacophore model of the binding of moderately large peptides to KRAS, we designed and synthesized an extensive and diverse library of small macrocyclic peptides. The need for the three key hydrophobic residues lends itself to being tackled by a peptide approach as the spatial disposition of their binding pockets requires a relatively large template not easily delivered by a conventional small molecule. Furthermore, given their hydrophobic nature, the need for three lipophilic binding groups would adversely affect the balance of physicochemical properties for a conventional small molecule, whereas overall properties are more balanced for a peptide. Additionally, the modular nature of peptide synthesis lends itself to the relatively simple synthesis of structurally complex compounds. Retaining the three key hydrophobic residues of the binding pharmacophore, early compounds were made where variations on the linker strategy were explored to identify a more synthetically tractable alternative to the thiol-propargyl linker originally employed. SAR analysis on the first library synthesized led us to identify 1,5-triazoles as the best linkers among those tested. This application of macrocyclization chemistry that used a small set of precursor residues to generate a wide range of linkers provided a successful and efficient demonstration of the utility of this type of approach to create diverse compound sets to screen for biologically active compounds.[20b] However, while strategically efficient in terms of the diversity achieved from a more limited range of starting materials, the macrocyclization chemistry did not deliver high yields in the formation of desired stapled, macrocyclic peptides. At best, yields were moderate, but more usually poor. A more detailed exploration and optimization of the key binding residues led to an extensive SAR study of the lipophilic pharmacophore triad, macrocycle size, and heteroatom incorporations *via* a one-point modification on the original structure. From these variations, we were able to discover several low micromolar inhibitors in compounds that were much simpler than the original, much larger peptides, thus supporting our initial hypothesis that it would be possible to retain RAS binding in peptides that have been "stripped down" to the core macrocyclic pharmacophore. Furthermore, the compounds synthesized during this work showed generally good physicochemical properties: reasonably drug-like lipophilicity and aqueous solubility. Additionally, in working with small peptides, the introduction of more conventionally un-drug-like lipophilic groups, such as naphthyl, did not so negatively impact such overall drug-like property measures. However, the most potent compounds found in this work were significantly less potent than the original larger peptides. Suspecting conformational influences, we used NMR to determine solution conformations for a number of examples. The observed SAR and conformational analysis appeared to suggest that this potency penalty is at least in part due to the compounds not showing a preferred conformation that appropriately presents the binding residues to interact with the RAS protein. Thus, we conclude that there is scope for further optimization of small macrocyclic inhibitors of this important biological target.

■ EXPERIMENTAL SECTION

HTRF Cyclic Peptide Competition Binding Assay on KRAS[G12V].[22] *Description.* Biotinylated KRAS[G12V] is mixed with streptavidin–europium and is preincubated in the plate with test compounds. An Alexa Fluor 647 labeled cyclic peptide is then added to the plate. Upon binding of the peptide to KRAS[G12V], the Alexa Fluor 647 (acceptor), a bright, far-red fluorescent dye, is brought into close proximity to the streptavidin–europium cryptate (donor) that is bound to the KRAS[G12V] via the biotin tag. FRET between the donor and the acceptor is then detected on a suitable plate reader (e.g., Envision or Pherastar). HTRF is used to reduce any background fluorescence. Molecules that inhibit the binding of the Alexa Fluor 647 labeled peptide will result in a reduced HTRF signal.

Protocol. Reagents were diluted in 20 mM HEPES, 150 mM NaCl, 5 mM MgCl$_2$, 0.01% Tween-20, and 1 mM DTT (base buffer). KRAS[G12V] was diluted to 4 nM in a base buffer containing 0.1 mg/mL bovine serum albumin (Sigma, A8577) and 20 ng/mL streptavidin europium (Cisbio, 610SAKLB). The Alexa Fluor 647 labeled peptide [1-[6-[6-[[(3R,6S,9S,12S,15S,18S,21S,24S,27S,30S,33S,36S,39S,42S,45S)-45-benzyl-9,30,39-tris(3-guanidinopropyl)-6,18-bis-(hydroxymethyl)-27-[(4-hydroxyphenyl)methyl]-15-(1H-indol-3-yl-methyl)-12,24,36,42-tetraisobutyl-21,33-diisopropyl-28-methyl-5,8,11,14,17,20,23,26,29,32,35,38,41,44,47-pentadecaoxo-1-thia-4,7,10,13,16,19,22,25,28,31,34,37,40,43,46-pentadecazacyclooctatetra-contane-3-carbonyl]amino]hexylamino]-6-oxo-hexyl]-2-[[(1E,3E,5E)-5-[3,3-dimethyl-5-sulfo-1-(3-sulfopropyl)indolin-2-ylidene]penta-1,3-dienyl]-3-methyl-3-(4-sulfobutyl)indol-1-ium-5-sulfonate] was diluted to 30 nM in a base buffer containing 0.1 M potassium fluoride. In a low-volume 384-well plate (Greiner 784904), 100 nL of the test compound in DMSO was dispensed using an Echo liquid handler (Labcyte, CA) and 5 μL of the KRas sample was added to all wells. After a 15 min preincubation, 5 μL of the Alexa Fluor 647 peptide was added to all wells. The plate was covered and incubated for 60 min at ambient temperature. The HTRF ratio was then measured using an excitation of 320 nm and dividing the emission at 665 nm by the emission at 620 nm multiplied by 10,000. Inhibition values were calculated from control DMSO wells (0% inhibition) and wells containing an excess of unlabeled peptide (100% inhibition). All data were analyzed using Genedata. The number of tests performed (n) for each compound is included in the Tables 4–6. These data are from generated independent experiments.

Ras/Raf Nucleotide Exchange HTRF assay.[22] Reagents were diluted in 20 mM HEPES, 150 mM NaCl, 5 mM MgCl2, 0.01% Tween-20, and 1 mM DTT. In a low-volume 384-well plate (Greiner 784904), 100 nL of the test compound in DMSO was dispensed using an Echo liquid handler (Labcyte, CA). Biotinylated-KRas[G12C]-GDP was premixed with streptavidin–europium (Cisbio, 610SAKLB) at 2× final assay concentrations (10 nM and 75 ng/mL, respectively), and 5 μL was added to the compound plate. The plate was covered to prevent evaporation.

In a separate reaction, GST-Raf was mixed with anti-GST XL665 (Cisbio, 61GSTXLA) at 2× final assay concentrations (20 nM and 4 μg/mL, respectively). The plate and the GST-Raf/Anti GST XL665 reactions were incubated at ambient temperature for 4 h to allow all reagents to equilibrate. SOS and GTPγS were then added to the GST-Raf/Anti GST-XL665 reaction to give a 2× final assay concentration (1 μM SOS and 2 μM GTPγS). The nucleotide exchange reaction

was initiated by adding 5 μL of the GST-Raf/Anti GST XL665, SOS, and GTPγS mixture to the assay plate. After a 1 h incubation at ambient temperature, the HTRF (homogeneous time-resolved fluorescence) ratio was measured using an excitation of 320 nm and dividing the emission at 665 nm by the emission at 620 nm multiplied by 10,000. Inhibition values were calculated from control DMSO wells (0% inhibition) and wells containing an excess of unlabeled peptide (100% inhibition). All data were analyzed using Genedata.

Chemistry. High-performance liquid chromatography (HPLC) was run on an Agilent 1260 Infinity machine using a Supelcosil ABZ + PLUS column (250 × 21.2 mm, 5 μm) with a linear gradient system (solvent A: 0.1% (v/v) TFA in water, solvent B: 0.05% (v/v) TFA in acetonitrile) over 20 min at a flow rate of 20 mL min^{-1}, visualized by UV absorbance (λmax = 254 nm). All final compounds were >95% pure by HPLC.

Standard magnetic resonance spectra (NMR) were recorded using an internal deuterium lock at ambient probe temperatures (unless otherwise stated) on Bruker DPX-400, Bruker Avance DRX-400, Bruker Avance 500 BB-ATM, and Bruker Avance 500 Cryo Ultrashield spectrometers.

High-resolution mass spectra (HRMS) were obtained with a Micromass Q-TOF mass spectrometer or a Waters LCT Premier Time of Flight mass spectrometer. Reported mass values are within the error limits of ±5 ppm mass units. Only molecular ions are reported using electrospray ionization technique.

Low-resolution mass spectra (LRMS) were recorded using liquid chromatography and mass spectroscopy (LCMS): Agilent 1200 series LC with an ESCi Multi-Mode Ionization Waters ZQ spectrometer using the MassLynx 4.0 software or Waters ACQUITY HClass UPLC with an ESCi Multi-Mode Ionization Waters SQ Detector 2 spectrometer using the MassLynx 4.1 software. Only molecular ions are reported using the electrospray ionization technique.

General procedures were adapted from those previous reported.[20] Macrocyclization reactions were carried out in standard glassware and using standard procedures.

General Procedure 1: Solid Supported Peptide Synthesis. The Rink Amide resin (0.1 mmol of supported amide, 1.0 equiv) was swelled in DMF (3 mL) for 30 min. After draining the solvent, the resin was deprotected with 20% piperidine solution in DMF (2 × 3 mL), shacking for 1 min. The resin was drained, and deprotection was checked by a Kaiser test. If successful, the resin was washed with DMF (3 × 3 mL), MeOH (3 × 3 mL), and DCM (3 × 3 mL). The Fmoc-protected amino acid of choice (0.2 mmol, 2.0 equiv) was premixed with HATU (0.2 mmol, 2.0 equiv) in DMF (3 mL) for 30 s. Then it was added to the resin, followed by DIPEA (0.4 mmol, 4.0 equiv), and the reaction mixture was stirred at room temperature for 3 min. After this time has passed, the resin was drained and washed with DMF (3 × 3 mL), MeOH (3 × 3 mL), and DCM (3 × 3 mL), and the coupling was checked *via* a Kaiser test. If the coupling was successful, the cycle was repeated starting from the deprotection until all desired amino acids have been coupled. The chemical yields and characterization of linear peptides prepared are detailed in Table S1 (Supporting Information).

General Cyclization Procedure A: Copper Mediated Azide–Alkyne Cycloaddition (1,4-Triazoles). A 1 mM solution of the linear peptide (1.0 equiv) in THF was degassed bubbling argon gas for 20 min. CuI (2.0 equiv) and DIPEA (4.0 equiv) were then added, and the reaction mixture was heated to reflux for 16 h under a nitrogen atmosphere. The solvent was removed by blowing nitrogen on the solution, and the residue was dissolved in MeCN and H_2O and purified with preparative HPLC (5 to 95% MeCN/H_2O over 20 min).

General Cyclization Procedure B: Ruthenium Catalyzed Azide–Alkyne Cycloaddition (1,5-Triazoles). A 1 mM solution of the linear peptide (1.0 equiv) in THF was degassed bubbling argon gas for 20 min. [Cp*RuCl]$_4$ (0.30 equiv) was then added, and the reaction mixture was heated to reflux for 16 h under a nitrogen atmosphere. The solvent was removed by blowing nitrogen on the solution, and the residue was dissolved in MeCN and H_2O and purified with preparative HPLC (5 to 95% MeCN/H_2O over 20 min).

General Cyclization Procedure B2: Ru-Catalyzed AACC for Full-Length Peptides (80, 81). A solution (0.8 mg/mL) of the linear peptide (1.0 equiv) in a H_2O/t-BuOH 1/1 mixture was degassed bubbling argon gas for 20 min. [Cp*RuCl]$_4$ (0.30 equiv) was then added, and the reaction mixture was stirred at room temperature for 16 h under a nitrogen atmosphere. The solvent was removed by blowing nitrogen on the solution, and the residue was dissolved in MeCN and H_2O and purified with preparative HPLC (5 to 95% MeCN/H_2O over 20 min).

General Cyclization Procedure C: Glaser Coupling. A 1 mM solution of the linear peptide (1.0 equiv) in MeOH was degassed bubbling argon gas for 20 min. Cu(OAc)$_2$ (2.0 equiv) and pyridine (4.0 equiv) were then added, and the reaction mixture was heated to 50 °C for 16 h under a nitrogen atmosphere. The solvent was removed by blowing nitrogen on the solution, and the residue was dissolved in MeCN and H_2O and purified with preparative HPLC (5 to 95% MeCN/H_2O over 20 min).

General Cyclization Procedure D: Ene–Yne metathesis. A 0.80 mM solution of the linear peptide (1.0 equiv) in DCM was degassed bubbling ethylene gas for 20 min. Grubbs' II Generation catalyst (0.20 equiv) was then added, and the reaction mixture was heated to reflux for 16 h under an ethylene gas atmosphere. The solvent was removed by blowing nitrogen on the solution, and the residue was dissolved in MeCN and H_2O and purified with preparative HPLC (5 to 95% MeCN/H_2O over 20 min).

General Cyclization Procedure E: Alkene Metathesis. A 0.37 mM solution of the linear peptide (1.0 equiv) in DCM was degassed bubbling argon gas for 20 min. Grubbs' II Generation catalyst (0.20 equiv) was then added, and the reaction mixture was heated to reflux for 16 h under a nitrogen atmosphere. The solvent was removed by blowing nitrogen on the solution, and the residue was dissolved in MeCN and H_2O and purified with preparative HPLC (5 to 95% MeCN/H_2O over 20 min).

General Cyclization Procedure F: Heck Coupling. A 0.50 mM solution of the linear peptide (1.0 equiv) in MeCN was degassed bubbling argon gas for 20 min. Pd(OAc)$_2$ (1.0 equiv) and K_2CO_3 (10.0 equiv) were then added, and the reaction mixture was heated to 50 °C for 16 h under a nitrogen atmosphere. The solvent was removed by blowing nitrogen on the solution, and the residue was dissolved in MeCN and H_2O and purified with preparative HPLC (5 to 95% MeCN/H_2O over 20 min).

The stapled peptides prepared by these methods, their chemical yields, and the MS and HPLC characterization are detailed in Table 2.

Conformational Analysis by NMR. All NMR spectra were recorded on a Bruker 500 MHz instrument equipped with a 5 mm QNP cryoprobe. Chemical shifts (δ values) are given in parts per million (ppm) and referenced to the H_2O residual signal (4.70 ppm). For the structural assignment of the macrocycles, 1D ^{1}H, 2D COSY, 2D TOCSY (mixing time 50 ms), 2D ROESY (mixing time 300 ms; relaxation delay 3 s), and ^{1}H–^{13}C HSQC spectra were acquired in both H_2O/D_2O (9:1) and 100% D_2O at 300 K using the standard pulse sequences available in TopSpin 4.0 (Bruker GmbH).

To determine the relative NOE intensities for pairs of spins, the extraction of F2-slices in the 2D ROESY at the F1-chemical shift of each resonance was carried out and the signals were then integrated.[25] To improve accuracy, the PANIC method (Peak Amplitude Normalization for Improved Cross-relaxation) was applied,[26] where the NOE intensities were normalized relative to the diagonal for each slice. Correction factors were then applied to compensate for the number of spins in each environment (corrected integral). For each molecule, the integral for two protons at a known distance was used as reference to calibrate the other interproton distances in the molecule using the equation below:[27]

$$\frac{\eta_{I1S}}{\eta_{I2S}} = \frac{r_{I1S}^{-6}}{r_{I2S}^{-6}}$$

where η_{IS} is the intensity of the NOE between I and S (S being the inverted spin) and r_{IS}^{-6} is the internuclear distance between I and S.

The sampling of the conformational space for the peptides was carried out with the Maestro Macrocycle Sampling algorithm using the OPLS3 force field (version 11.6.013, Schrödinger) with an energy threshold of 25 kcal/mol to allow a full exploration of the rotation around the peptidic bonds. The NMR restraints were collected in the form of NOEs and J couplings. Additional no-NOE constraints (between protons not showing cross-peaks in the ROESY) were also used at a default distance of 4.5 Å. The MSpin NOE Fitter[27] algorithm (version 2.4.0-713; MestReLab Research) was utilized to select the conformers generated with Maestro that best agreed with the NMR experimental data. MSpin selected seven different conformations, and these ones were subjected to solvent explicit MD simulations (Desmond Molecular Dynamics software module, D.E. Shaw, v4.4, running inside Maestro) using 10 ns in length runs with energy value recording every 1.2 ps and trajectory recording every 4.8 ps. The trajectories were then RMSD clustered using the Clustering tool in Maestro, and the most populated cluster was taken as the conformation in which the molecule spent most time in the dynamics run. The most populated cluster for each of the initial seven conformations was compared with the NMR restraints, and the best fit was selected as the probable conformer in the solution.

Preparation of Novel Intermediates.
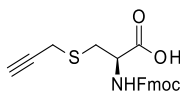
N-Fmoc-S-propargyl-ʟ-cysteine (I_1). A solution of *S*-propargyl-ʟ-cysteine (10.0 g, 62.8 mmol, 1.0 equiv) and $NaHCO_3$ (15.8 g, 188.4 mmol, 3 equiv) in H_2O (90 mL) was stirred at room temperature until clear. Then, a solution of Fmoc-ONSu (21.2 g, 62.8 mmL, 1.0 equiv) in MeCN (90 mL) was added and stirred for 16 h. The reaction was quenched with HCl 1 N, bringing the pH to 1, and then extracted with EtOAc (6 × 100 mL). The organic layers were combined and dried over $MgSO_4$, and solvents were removed *in vacuo* to yield a brown oil crude. This was purified by FCC (gradient from 100% DCM to DCM/MeOH 20:1) to yield a foamy, pink solid. This was dissolved in the minimum amount of warm DCM and precipitated by the addition of cold hexane. The white solid thus formed was collected by filtration, washed with cold Et_2O, and dried (18.8 g, 49.3 mmol, 78%).

^1H NMR (400 MHz, $CDCl_3$) δ 2.25 (d, J = 2.4 Hz, 1H), 3.08–3.39 (m, 4H), 4.24 (t, J = 6.7 Hz, 1H), 4.45 (d, J = 6.6 Hz, 2H), 4.64–4.76 (m, 1H), 5.64 (d, J = 7.3 Hz, 1H), 7.32 (t, J = 7.4 Hz, 2H), 7.41 (t, J = 7.4 Hz, 2H), 7.60 (d, J = 6.8 Hz, 2H), 7.77 (d, J = 7.5 Hz, 2H); ^{13}C NMR (151 MHz, $CDCl_3$) 173.3, 156.0, 143.7, 143.5, 127.6, 127.0, 125.0, 120.0, 79.3, 72.0, 67.1, 53.4, 47.0, 33.7, 19.9; LCMS (ESI, M + H$^+$) m/z = 382.3.
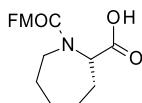
(S)-N-Fmoc-azepane-2-carboxylic Acid (I_2). To a solution of (2*S*)-azepane-2-carboxylic acid (350 mg, 2.44 mmol, 1.0 equiv) in H_2O (5 mL) was added K_2CO_3 (680 mg) to bring the pH to 10. A solution of Fmoc-ONSu (895 mg, 2.93 mmol, 1.2 equiv) in 1,4-dioxane (5 mL) was then added, and the reaction mixture was stirred for 18 h. The volume was then reduced *in vacuo* and diluted with a mixture of H_2O/EtOAc, and the layers were separated. The aqueous solution was further washed with EtOAc (5 mL), and the organic layers set aside; the aqueous layer was acidified to pH 1 using 6 N HCl and then extracted with EtOAc (3 × 10 mL). The organic extracts were combined, washed with brine (10 mL), and dried over $MgSO_4$; the solvent was removed *in vacuo*; and the resulting crude was recrystallized from Et_2O and hexane to yield the title compound as a white solid (190 mg, 0.52 mmol, 48%).

Mixture of rotamers. ^1H NMR (400 MHz, $CDCl_3$) 1.15–1.97 (m, 7H), 2.24–2.46 (m, 1H), 2.9–3.04 (m, 1H), 3.77–3.9 (m, 0.5H), 4.01 (d, J = 14.4 Hz, 0.5H), 4.20 (t, J = 6.1 Hz, 0.5H), 4.27 (t, J = 6.5 Hz, 0.5H), 4.33–4.58 (m, 2.5H), 4.65 (dd, J = 12.1, 6.2 Hz, 0.5H),

7.18–7.46 (m, 4H), 7.47–7.67 (m, 2H), 7.65–7.84 (m, 2H), 9.22 (br s, 1H); LCMS (ESI, [M + H$^+$]) m/z = 366.

■ ASSOCIATED CONTENT

ⓈⒾ Supporting Information

The Supporting Information is available free of charge at https://pubs.acs.org/doi/10.1021/acs.jmedchem.1c01334.

> Abbreviation index, linear peptide yields and data, lead compound HPLC traces, NMR conformational analysis data, NMR spectra of novel intermediates, molecular dynamics results, references for the synthesis of known starting materials, and Molecular Formula Strings (PDF)

■ AUTHOR INFORMATION

Corresponding Authors

Andrew P. Thomas − *Chemistry, Oncology R&D, AstraZeneca, Cambridge CB4 0WG, U.K.;* ⓞ orcid.org/0000-0003-3385-8903; Phone: +44 1223 223570; Email: andrew.p.thomas@atrazenenca.com

David R. Spring − *Department of Chemistry, Cambridge University, Cambridge CB2 1EW, U.K.;* ⓞ orcid.org/0000-0001-7355-2824; Phone: +44 1223 336498; Email: spring@ch.cam.ac.uk

Authors

Gabriele Fumagalli − *Department of Chemistry, Cambridge University, Cambridge CB2 1EW, U.K.; Chemistry, Oncology R&D, AstraZeneca, Cambridge CB4 0WG, U.K.;* Present Address: Domainex Ltd., Chesterford Research Park, Saffron WaldenAQ10: Please check if data inserted here is correct. CB10 1XL, U.K

Rodrigo J. Carbajo − *Chemistry, Oncology R&D, AstraZeneca, Cambridge CB4 0WG, U.K.;* Present Address: Discovery Sciences In Silico Discovery & External Innovation, Janssen Research and Development, C/Rio Jarama, 75A-45007 Toledo, Spain.; ⓞ orcid.org/0000-0002-0312-6499

J. Willem M. Nissink − *Chemistry, Oncology R&D, AstraZeneca, Cambridge CB4 0WG, U.K.;* ⓞ orcid.org/0000-0003-2572-9140

Jonathan Tart − *Discovery Sciences, BioPharmaceuticals R&D, AstraZeneca, Cambridge CB4 0WG, U.K.*

Rongxuan Dou − *Department of Chemistry, Cambridge University, Cambridge CB2 1EW, U.K.*

Complete contact information is available at:
https://pubs.acs.org/10.1021/acs.jmedchem.1c01334

Author Contributions

The manuscript was written through contributions of all authors. All authors have given approval to the final version of the manuscript.

Notes

The authors declare no competing financial interest.

■ ACKNOWLEDGMENTS

and Chris Phillips and Jason Breed for the attempted crystallography.

ABBREVIATIONS

all amino acids, standard one- or three-letter codes; AACC, azide−alkyne click chemistry; DTT, dithiothreitol; FRET, fluorescence resonance energy transfer; HEPES, 4-(2-hydroxyethyl)-1-piperazineethanesulfonic acid;; HTRF, homogeneous time-resolved fluorescence; SAR, structure−activity relationship; SPPS, solid-phase peptide synthesis

REFERENCES

(1) Bivona, T. G.; Quatela, S. E.; Bodemann, B. O.; Ahearn, I. M.; Soskis, M. J.; Mor, A.; Miura, J.; Wiener, H. H.; Wright, L.; Saba, S. G.; Yim, D.; Fein, A.; Pérez de Castro, I.; Li, C.; Thompson, C. B.; Cox, A. D.; Philips, M. R. PKC regulates a farnesyl-electrostatic switch on K-Ras that promotes its association with Bcl-XL on mitochondria and induces apoptosis. *Mol. Cell* **2006**, *21*, 481−493.

(2) Steelman, L. S.; Franklin, R. A.; Abrams, S. L.; Chappell, W.; Kempf, C. R.; Bäsecke, J.; Stivala, F.; Donia, M.; Fagone, P.; Nicoletti, F.; Libra, M.; Ruvolo, P.; Ruvolo, V.; Evangelisti, C.; Martelli, A. M.; McCubrey, J. A. Roles of the Ras/Raf/MEK/ERK pathway in leukemia therapy. *Leukemia* **2011**, *25*, 1080−1094.

(3) Stephen, A. G.; Esposito, D.; Bagni, R. K.; McCormick, F. Dragging Ras back in the ring. *Cancer Cell* **2014**, *25*, 272−281.

(4) Prior, I. A.; Lewis, P. D.; Mattos, C. A comprehensive survey of Ras mutations in cancer. *Cancer Res.* **2012**, *72*, 2457−2467.

(5) (a) Downward, J. Targeting RAS signalling pathways in cancer therapy. *Nat. Rev. Cancer* **2003**, *3*, 11−22. (b) Wang, W.; Fang, G.; Rudolph, J. Ras inhibition via direct Ras binding − is there a path forward? *Bioorg. Med. Chem. Lett.* **2012**, *22*, 5766−5776. (c) Mao, Y.; Yao, H.; Wang, H.; Cheng, P.; Long, D. Microsecond timescale dynamics of GDP-bound Ras underlies the formation of novel inhibitor-binding pockets. *Angew. Chem.* **2016**, *55*, 15629−15632. (d) Müller, M. P.; Jeganathan, S.; Heidrich, A.; Campos, J.; Goody, R. S. Nucleotide based covalent inhibitors of KRas can only be efficient in vivo if they bind reversibly with GTP-like affinity. *Sci. Rep.* **2017**, *7*, 3687.

(6) (a) Ostrem, J. M.; Peters, U.; Sos, M. L.; Wells, J. A.; Shokat, K. M. K-Ras(G12C) inhibitors allosterically control GTP affinity and effector interactions. *Nature* **2013**, *503*, 548−551. (b) Hansen, R.; Peters, U.; Babbar, A.; Chen, Y.; Feng, J.; Janes, M. R.; Li, L.-S.; Ren, P.; Liu, Y.; Zarrinkar, P. P. The reactivity-driven biochemical mechanism of covalent KRAS G12C inhibitors. *Nat. Struct. Mol. Biol.* **2018**, *25*, 454−462. (c) Goody, R. S.; Müller, M. P.; Rauh, D. Mutant-specific targeting of Ras G12C activity by covalently reacting small molecules. *Cell Chem. Biol.* **2019**, *26*, 1338−1348. (d) Lanman, B. A.; Allen, J. R.; Allen, J. G.; Amegadzie, A. K.; Ashton, K. S.; Booker, S. K.; Chen, J. J.; Chen, N.; Frohn, M. J.; Goodman, J.; Kopecky, D. J.; Liu, L.; Lopez, P.; Low, J. D.; Ma, V.; Minatti, A. E.; Nguyen, T. T.; Nishimura, N.; Pickrell, A. J.; Reed, A. B.; Shin, Y.; Siegmund, A. C.; Tamayo, N. A.; Tegley, C. M.; Walton, M. C.; Wang, H.-L.; Wurz, R. P.; Xue, M.; Yang, K. C.; Achanta, P.; Bartberger, M. D.; Canon, J.; Hollis, L. S.; McCarter, J. D.; Mohr, C.; Rex, K.; Saiki, A. Y.; San Miguel, T.; Volak, L. P.; Wang, K. H.; Whittington, D. A.; Zech, S. G.; Lipford, J. R.; Cee, V. J. Discovery of a covalent inhibitor of KRASG12C (AMG 510) for the treatment of solid tumors. *J. Med. Chem.* **2020**, *63*, 52−65.

(7) (a) Kessler, D.; Gmachl, M.; Mantoulidis, A.; Martin, L. J.; Zoephel, A.; Mayer, M.; Gollner, A.; Covini, D.; Fischer, S.; Gerstberger, T.; Gmaschitz, T.; Goodwin, C.; Greb, P.; Häring, D.; Hela, W.; Hoffmann, J.; Karolyi-Oezguer, J.; Knesl, P.; Kornigg, S.; Koegl, M.; Kousek, R.; Lamarre, L.; Moser, F.; Munico-Martinez, S.; Peinsipp, C.; Phan, J.; Rinnenthal, J.; Sai, J.; Salamon, C.; Scherbantin, Y.; Schipany, K.; Schnitzer, R.; Schrenk, A.; Sharps, B.; Siszler, G.; Sun, Q.; Watersond, A.; Wolkerstorfer, B.; Zeeb, M.; Pearson, M.; Fesik, S. W.; McConnell, D. B. Drugging an undruggable pocket on KRAS. *Proc. Natl. Acad. Sci. U. S. A.* **2019**, *116*, 15823−15829.

(b) Tran, T. H.; Alexander, P.; Dharmaiah, S.; Agamasu, C.; Nissley, D. V.; McCormick, F.; Esposito, D.; Simanshu, D. K.; Stephen, A. G.; Balius, T. E. The small molecule BI-2852 induces a nonfunctional dimer of KRAS. *Proc. Natl. Acad. Sci. U. S. A.* **2020**, *117*, 3363−3364.

(8) (a) Sogabe, S.; Kamada, Y.; Miwa, M.; Niida, A.; Sameshima, T.; Kamaura, M.; Yonemori, K.; Sasaki, S.; Sakamoto, J.; Sakamoto, K. Crystal structure of a human K-Ras G12D mutant in complex with GDP and the cyclic inhibitory peptide KRpep-2d. *ACS Med. Chem. Lett.* **2017**, *8*, 732−736. (b) Niida, A.; Sasaki, S.; Yonemori, K.; Sameshima, T.; Yaguchi, M.; Asami, T.; Sakamoto, K.; Kamaura, M. Investigation of the structural requirements of K-Ras(G12D) selective inhibitory peptide KRpep-2d using alanine scans and cysteine bridging. *Bioorg. Med. Chem. Lett.* **2017**, *27*, 2757−2761. (c) Sakamoto, K.; Kamada, Y.; Sameshima, T.; Yaguchi, M.; Niida, A.; Sasaki, S.; Miwa, M.; Ohkubo, S.; Sakamoto, J.; Kamaura, M.; Cho, N.; Tani, A. K-Ras(G12D)-selective inhibitory peptides generated by random peptide T7 phage display technology. *Biochem. Biophys. Res. Commun.* **2017**, *484*, 605−611.

(9) Moore, A. R.; Rosenberg, S. C.; McCormick, F.; Malek, S. RAS-targeted therapies: is the undruggable drugged? *Nat. Rev. Drug Discovery* **2020**, *19*, 533−552.

(10) Sakamoto, K.; Masutani, T.; Hirokawa, T. Generation of KS-58 as the first K-Ras-(G12D)-inhibitory peptide presenting anti-cancer activity in vivo. *Sci. Rep.* **2020**, *10*, 21671.

(11) Jackson, R.; Waring, M.; Hudson, K.; Phillips, C. *unpublished results*

(12) (a) Uhlig, T.; Kyprianou, T.; Martinelli, F. G.; Oppici, C. A.; Heiligers, D.; Hills, D.; Calvo, X. R.; Verhaert, P. The emergence of peptides in the pharmaceutical business: from exploration to exploitation. *EuPa Open Proteomics* **2014**, *4*, 58−69. (b) Fosgerau, K.; Hoffmann, T. Peptide therapeutics: current status and future directions. *Drug Discovery Today* **2015**, *20*, 122−128.

(13) (a) Antosova, Z.; Mackova, M.; Kral, V.; Macek, T. Therapeutic application of peptides and proteins: parenteral forever? *Trends Biotechnol.* **2009**, *27*, 628−635. (b) Pichereau, C. A. A. C.; Allary, C. Therapeutic peptides under the spotlight. *Eur. Biopharm.* **2005**, *5*, 88−91. (c) Langer, R.; Lund, D.; Leong, K.; Folkman, J. Controlled release of macromolecules: Biological studies. *J. Controlled Release* **1985**, *2*, 331−341.

(14) (a) Geotti-Bianchini, P.; Moretto, A.; Peggion, C.; Beyrath, J.; Bianco, A.; Formaggio, F. Replacement of Ala by Aib improves structuration and biological stability in thymine-based α-nucleopeptides. *Org. Biomol. Chem.* **2010**, *8*, 1315−1321. (b) Garton, M.; Nim, S.; Stone, T. A.; Wang, K. E.; Deber, C. M.; Kim, P. M. Method to generate highly stable D-amino acid analogs of bioactive helical peptides using a mirror image of the entire PDB. *Proc. Natl. Acad. Sci. U. S. A.* **2018**, *115*, 1505−1510. (c) El-Sayed, A.; Futaki, S.; Harashima, H. *AAPS J.* **2009**, *11*, 13−22. (d) Wender, P. A.; Galliher, W. C.; Goun, E. A.; Jones, L. R.; Pillow, T. H. The design of guanidinium-rich transporters and their internalization mechanisms. *Adv. Drug Delivery Rev.* **2008**, *60*, 452−472.

(15) Iegre, J.; Gaynord, J. S.; Robertson, N. S.; Sore, H. F.; Hyvönen, M.; Spring, D. R. Two-component stapling of biologically active and conformationally constrained peptides: past, present, and future. *Adv. Ther.* **2018**, 1800052 , and references therein.

(16) Robertson, N. S.; Spring, D. R. Using peptidomimetics and constrained peptides as valuable tools for inhibiting protein-protein interactions. *Molecules* **2018**, *23*, 959. , and references therein

(17) Blackwell, H. E.; Grubbs, R. H. Highly efficient synthesis of covalently cross-linked peptide helices by ring-closing metathesis. *Angew. Chem., Int. Ed.* **1998**, *37*, 3281−3284.

(18) Schafmeister, C. E.; Po, J.; Verdine, G. L. An all-hydrocarbon cross-linking system for enhancing the helicity and metabolic stability of peptides. *J. Am. Chem. Soc.* **2000**, *122*, 5891−5892.

(19) Chorev, M.; Roubini, E.; McKee, R. L.; Gibbons, S. W.; Goldman, M. E.; Caulfield, M. P.; Rosenblatt, M. Cyclic parathyroid hormone-related protein antagonists: Lysine 13 to aspartic acid 17 [i to (i+4)] side chain to side chain lactamization. *Biochemistry* **1991**, *30*, 5968−5974.

(20) (a) Beckmann, H. S. G.; Nie, F.; Hagerman, C. E.; Johansson, H.; Tan, Y. S.; Wilcke, D.; Spring, D. R. A strategy for the diversity-oriented synthesis of macrocyclic scaffolds using multidimensional coupling. *Nat. Chem.* **2013**, *5*, 861−867. (b) Nie, F.; Kunciw, D. L.; Wilcke, D.; Stokes, J. E.; Galloway, W. R. J. D.; Bartlett, S.; Sore, H. F.; Spring, D. R. A multidimensional diversity-oriented synthesis strategy for structurally diverse and complex macrocycles. *Angew. Chem., Int. Ed.* **2016**, *55*, 11139−11143.

(21) (a) Williams, R. M.; Sinclair, P. J.; Zhai, D.; Chen, D. Practical asymmetric syntheses of. alpha.-amino acids through carbon-carbon bond constructions on electrophilic glycine templates. *J. Am. Chem. Soc.* **1988**, *110*, 1547−1557. (b) Dutton, F. E.; Lee, B. H.; Johnson, S. S.; Coscarelli, E. M.; Lee, P. H. Restricted conformation analogues of an anthelmintic cyclodepsipeptide. *J. Med. Chem.* **2003**, *46*, 2057−2073.

(22) The Ras biochemical coupled assay was an adaptation of the HTRF assay described in: Winter, J. J.; Anderson, M.; Blades, K.; Brassington, C.; Breeze, A. L.; Chresta, C.; Embrey, K.; Fairley, G.; Faulder, P.; Finlay, M. R.; Kettle, J. G.; Nowak, T.; Overman, R.; Patel, S. J.; Perkins, P.; Spadola, L.; Tart, J.; Tucker, J. A.; Wrigley, G. Small molecule binding sites on the Ras:SOS complex can be exploited for inhibition of Ras activation. *J. Med. Chem.* **2015**, *58*, 2265−2274.

(23) Balazs, A. Y. S.; Carbajo, R. J.; Davies, N. L.; Dong, Y.; Hird, A. W.; Johannes, J. W.; Lamb, M. L.; McCoull, W.; Raubo, P.; Robb, G. R.; Packer, M. J.; Chiarparin, E. Free ligand 1D NMR conformational signatures to enhance structure based drug design of a Mcl-1 inhibitor (AZD5991) and other synthetic macrocycles. *J. Med. Chem.* **2019**, *62*, 9418−9437.

(24) Appavoo, S. D.; Huh, S.; Diaz, D. B.; Yudin, A. K. Conformational control of macrocycles by remote structural modification. *Chem. Rev.* **2019**, *119*, 9724−9752.

(25) Butts, C. P.; Jones, C. R.; Towers, E. C.; Flynn, J. L.; Appleby, L.; Barron, N. J. Interproton distance determinations by NOE − surprising accuracy and precision in a rigid organic molecule. *Org. Biomol. Chem.* **2011**, *9*, 177−184.

(26) (a) Macur, S.; Farmer, B. T.; Brown, L. R., II Communication An improved method for the determination of cross-relaxation rates from NOE data. *J. Magn. Reson.* **1986**, *70*, 493−499. (b) Hu, H.; Krishnamurthy, K. Revisiting the initial rate approximation in kinetic NOE measurements. *J. Magn. Reson.* **2006**, *182*, 173−177.

(27) Troche-Pesqueira, E.; Anklin, C.; Gil, R. R.; Navarro-Vázquez, A. Computer assisted 3D structure elucidation of natural products using residual dipolar couplings. *Angew. Chem., Int. Ed.* **2017**, *56*, 3660−3664.